

Response to Anonymous Referee #2

This manuscript attempts to estimate dBC/dCO ratios from long period observations in Asia and use them to evaluate the BC/CO ratio in emission inventory. The measurements are interesting to the community and valuable for improving the understanding of BC emission. However, several points need to be clarified before the manuscript is accepted for publication.

Response: We thank the reviewer for carefully reviewing the manuscript and providing valuable comments. For convenience, your comments are italicized and numbered. The line (L) numbers in the responses correspond to those in the revised manuscript. The changes in the revised manuscript are underlined in the responses as necessary and are indicated as ‘tracked changes’ in the manuscript.

General Comments:

1. *As described in Section 2.3, dCO was calculated by subtracting the baseline level (determined as a 14-day moving 5th percentile) from the observed CO , dBC was calculated as BC concentration as the baseline was assumed to be zero. These assumptions are important for all the analyses in this work, however, the authors did not provide any explanation for using them. Is there any studies/data that can support these assumptions?*

We added the reason why we assumed the BC baseline as zero as follows:

“On the other hand, ΔBC is the BC concentration as is (BC baseline = 0), because the ~~baseline concentration was assumed~~ atmospheric lifetime of BC is estimated to be zero; several days (Park et al., 2005), in contrast to that of CO , which has a one- or two-month lifetime (Bey et al. 2001).” (L203-206)

We tried to discuss the CO baseline estimation in detail as follows:

“ ΔCO was calculated by subtracting the baseline level (~~determined as a 14-day moving 5th percentile~~) from the observed CO mixing ratio. Though there are several methods for estimating the CO baseline level (e.g., Matsui et al., 2011; Miyakawa et al. 2017; Oshima et al., 2012; Verma et al. 2011), the CO baseline in this study was regarded as a 14-day moving 5th percentile based on Kanaya et al. (2016).” (L199-203)

“The uncertainty of the BC/CO ratio that may arise from estimating the CO baseline by different methods and from allocation methods involving selecting different altitudes are discussed in the Supplement (S4).” (L227-229)

In supplement (S4), we added a paragraph and figure as follows:

“First, there are several ways to determine the CO baseline, mainly depending on the measurement period. For intensive measurement periods, the CO baseline can be calculated from the 5th percentile of data

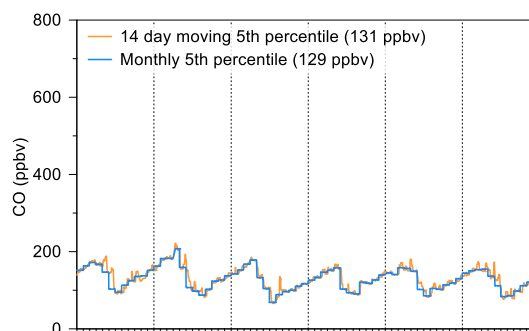


Figure S5. Time series of CO baselines calculated by different methods (14-day moving 5th and monthly 5th percentiles) at Noto.

(Matsui et al. 2011; Miyakawa et al., 2017) or the x-intercept of the best-fit line between BC and CO (Oshima et al., 2012). It can also be calculated by the 5th percentile of the CO concentration from monthly (Verma et al. 2011) or moving 14-day (Kanaya et al. 2016) from long-term measurements. We tested the difference in CO baselines calculated from the 5th percentile of the moving 14-day (our method) and monthly CO data (Figure S5). The difference in the CO baseline from the monthly data was slightly lower (-2 ppbv; -1.9%) than our estimation. Moreover, the mean $\Delta BC/\Delta CO$ ratios from the two different methods did not show significant differences (5.82 ng m⁻³ ppb⁻¹ for our estimation and 5.87 ng m⁻³ ppb⁻¹ for monthly data), when Welch's t-test was applied ($p > 0.1$)."

Bey, I., Jacob, D., Logan, J., and Yantosca, R.: Asian chemical outflow to the Pacific in spring: Origins, pathways, and budgets, *J. Geophys. Res.-Atmos.*, 106, 23097–23113, doi:10.1029/2001JD000806, 2001

Park, R. J., Jacob, D. J., Palmer, P. I., Clarke, A. D., Weber, R. J., Zondlo, M. A., Eisele, F. L., Bandy, A. R., Thornton, D. C., Sachse, G.W., and Bond, T. C.: Export efficiency of black carbon aerosol in continental outflow: Global implications, *J. Geophys. Res.-Atmos.*, 110, 1–7, <https://doi.org/10.1029/2004JD005432>, 2005.

Matsui, H., Kondo, Y., Moteki, N., Takegawa, N., Sahu, L. K., Zhao, Y., Fuelberg, H. E., Sessions, W. R., Diskin, G., Blake, D. R., Wisthaler, A., and Koike, M.: Seasonal variation of the transport of black carbon aerosol from the Asian continent to the Arctic during the ARCTAS aircraft campaign, *Journal of Geophysical Research: Atmospheres*, 116, 10.1029/2010JD015067, 2011.

2. *A large part of this manuscript is using the dBC/dCO to validate REAS emission inventory. However, there is no introduction for REAS in the manuscript. The authors need to provide some key information for this inventory. e.g. What years does it cover? What is the resolution of this inventory? Is there any seasonal/diurnal variation included in the inventory? How is it compared with other inventories? Any studies have evaluated the inventory?*

We are sorry for providing insufficient information on the REAS v2.1 inventory, though we tried to mention the key reference. We added brief information on REAS v2.1 and references as follows:

"... Regional Emission inventory in ASia (REAS) version 2.1 based on the 2008 emission inventory (Kurokawa et al., 2013) of BC and CO with sufficient spatio-temporal coverage. The REAS inventory comprises emissions data from 30 Asian countries and regions, including China, North Korea, South Korea and Japan, between the years 2000 and 2008 at a 0.25°×0.25° horizontal resolution. The emissions sources consisted of power plants, combustible and non-combustible sources in industry, on-road and off-road sources in transport, and residential and other activities, such as agricultural activities and evaporative sources (Han et al., 2015; Itahashi et al., 2017; Kurokawa et al., 2013; Saikawa et al., 2017; Uno et al., 2017)." (L89-97)

Han, K. M., Lee, S., Chang, L. S., and Song, C. H.: A comparison study between CMAQ-

simulated and OMI-retrieved NO₂ columns over East Asia for evaluation of NO_x emission fluxes of INTEX-B, CAPSS, and REAS inventories, *Atmos. Chem. Phys.*, 15, 1913-1938, 10.5194/acp-15-1913-2015, 2015.

Saikawa, E., Kim, H., Zhong, M., Avramov, A., Zhao, Y., Janssens-Maenhout, G., Kurokawa, J.-I., Klimont, Z., Wagner, F., Naik, V., Horowitz, L. W., and Zhang, Q.: Comparison of emissions inventories of anthropogenic air pollutants and greenhouse gases in China, *Atmos. Chem. Phys.*, 17, 6393–6421, <https://doi.org/10.5194/acp-17-6393-2017>, 2017.

Specific comments:

3. *Line 142: The statement of the updated MAC showed perfect correlation with COSMOS is not useful, since COSMOS also relies on assumed MAC. In addition, MAC could vary largely among different locations/periods. The key question here is whether MAAP measurements at these 2 sites are consistent with those measured by thermal optical method. Have the authors done any comparisons between MAAP and OC-EC analyzer BC?*

COSMOS is a filter photometer specially equipped with a pre-heater to remove co-existing non-refractory species, and its reliable performance has been demonstrated against SP2 and EC/OC (Miyakawa et al., 2017; Kondo et al., 2011; Ohata et al., 2019), serving as a central instrument for harmonization. Therefore, we added more detailed descriptions and relevant references as follows:

“... reported to have good agreement between instruments, including OC-EC analyzers (Sunset Laboratory Inc., USA) with optical corrections, single-particle soot photometers (SP2), continuous soot-monitoring systems (COSMOS) and multi-angle absorption photometers (MAAP 5012 Thermo Scientific) (e.g., Kondo et al., 2011; Kanaya et al., 2008, 2013, 2016; Miyakawa et al., 2016, 2017; Taketani et al., 2016; Ohata et al., 2019).” (L132-136)

“It should be noted that we used a different mass absorption efficiency (MAE) value of 10.3 m² g⁻¹, as suggested by Kanaya et al. (2013), instead of the default MAE of 6.6 m² g⁻¹, which showed perfect correlation with the COSMOS BC concentration (Kanaya et al., 2013). This value was validated with COSMOS, which showed a reliable performance with SP2 and OC-EC analyzer (Miyakawa et al., 2017; Kondo et al., 2011; Ohata et al., 2019) on a long-term basis at Fukue (Kanaya et al., 2016) and in Tokyo (Kanaya et al., 2013). The consistency between MAAP and SP2 at Noto was reported at ~10% (Taketani et al., 2016). At Fukuoka, a similar behavior was expected as the BC there would be a mixture from the continent and urban sources, as experienced at Fukue and Tokyo.” (L150-158)

Kondo, Y., Sahu, L., Moteki, N., Khan, F., Takegawa, N., Liu, X., Koike, M., and Miyakawa, T.: Consistency and Traceability of Black Carbon Measurements Made by Laser-Induced Incandescence, Thermal-Optical Transmittance, and Filter-Based Photo-Absorption Techniques, *Aerosol Sci. Tech.*, 45, 295-312, 10.1080/02786826.2010.533215, 2011.

Miyakawa, T., Kanaya, Y., Komazaki, Y., Taketani, F., Pan, X., Irwin, M., and Symonds,

J.: Intercomparison between a single particle soot photometer and evolved gas analysis in an industrial area in Japan: Implications for the consistency of soot aerosol mass concentration measurements, *Atmos. Environ.*, 127, 14-21, <https://doi.org/10.1016/j.atmosenv.2015.12.018>, 2016.

Ohata, S., Kondo, Y., Moteki, N., Mori, T., Yoshida, A., Sinha, P. R., and Koike, M.: Accuracy of black carbon measurements by a filter-based absorption photometer with a heated inlet, *Aerosol Sci. Tech.*, 53, 1079-1091, 10.1080/02786826.2019.1627283, 2019.

Taketani, F., Kanaya, Y., Nakayama, T., Ueda, S., Matsumi, Y., Sadanaga, Y., Iwamoto, Y., and Matsuki, A.: Property of Black Carbon Particles Measured by a Laser-Induced Incandescence Technique in the spring at Noto Peninsula, Japan, *J. Aerosol Res.*, 31, 194-202, 10.11203/jar.31.194, 2016 (Abstract in English).

4. *Line 159: The slope of 1.17 looks not small for this study. I would suggest the authors add a short discussion for the uncertainties of their all measurements, and discuss how those uncertainties may affect their results and conclusions.*

The uncertainties of the sunset EC/OC (L144) and MAAP (L160) were already mentioned, so we added the uncertainties of the BC and CO measurements as follows:

“The overall uncertainties of the BC and CO measurements were estimated to be less than 15% (except for Gosan, at 20%) and 5%, respectively. The overall regional $\Delta BC/\Delta CO$ ratio varied from -0.7 (-8%) to 0.8 (10%) due to uncertainty.” (L177-180)

5. *Section 3.3: As mentioned above, the authors need to give an introduction for the REAS v2.1 inventory. The key question is whether REAS covers the measurement period and reflects current emission inventory knowledge. If it is possible, I strongly suggest the authors to compare their measured dBC/dCO with more inventories (e.g. MIX). This may provide some insight for identifying the bias source of emission inventories.*

Though the time periods of the measurements and the REAS emission inventory were different, the long-term variation of the $\Delta BC/\Delta CO$ ratio did not show changes in the trends at a significant level ($p \geq 0.1$), and the results of the BC/CO ratio from the EDGAR emission inventory from 2008 to 2012 and the MIX emission inventory in 2008 and 2010 coincided. Therefore, we added relevant analysis as follows:

“It should be noted that there were no significant changes in trends for the long-term variation of the $\Delta BC/\Delta CO$ ratios of all sites, as well as BC/CO ratios from the Emissions Database for Global Atmospheric Research (EDGAR version 4.3.2; Crippa et al. 2018) emission inventory since 2008 and the MIX emission inventory (Li et al., 2017) in 2008 and 2010 (Figure S6). This result implied that comparison between the measurements and the REAS emission inventory was a reasonable approach, even though the time scale between them did not match.” (L278-284)

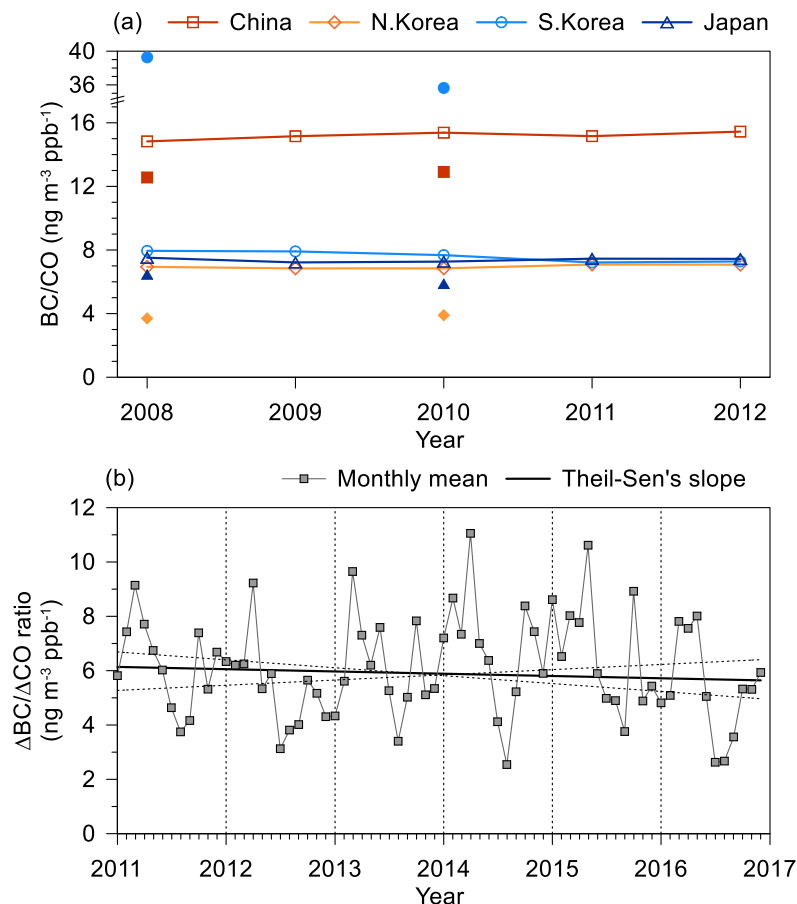


Figure S6. (a) Time series of the BC/CO ratios from the Emissions Database for Global Atmospheric Research (EDGAR v4.3.2; open symbols) during 2008 – 2012 and MIX emission inventory (filled symbols) in 2008 and 2010. (b) Time series of the monthly means of the $\Delta BC/\Delta CO$ ratio with Theil-Sen's slope during the measurement periods at Noto. The Theil-Sen's slope of the $\Delta BC/\Delta CO$ ratio indicated a slight decreasing trend of the $\Delta BC/\Delta CO$ ratio at $-0.08/\text{year}$; but the trend was statistically insignificant ($p > 0.1$). Insignificant trends of the $\Delta BC/\Delta CO$ ratio were also observed at the other sites.

Although the main purpose of this manuscript is verification of the REAS emission inventory (L87-91), we added a discussion about the regional and seasonal variation in the EDGAR and MIX emission inventories without losing the focus on the REAS inventory as follows:

“In the case of the MIX emission inventory, the emission rates from North and South Korea were derived from the REAS and CAPSS inventories, respectively, and both the emission rates and BC/CO ratio were within a narrow range of those of the REAS inventory. However, for EDGAR, while the BC/CO ratios in North Korea, South Korea, and Japan were relatively consistent with the ratios from measurements, the overestimation for China was remarkable compared to both the measurement ratios and other emission inventories. Especially, North China showed the highest BC/CO ratio compared to East and Northeast China, because the industry sector in North China has the largest BC and CO emission rates

(63% and 35% of total, respectively), along with a high BC/CO ratio ($38.5 \text{ ng m}^{-3} \text{ ppb}^{-1}$).” (L416-424)

“Similar to the regional variation, the seasonal variation of other inventories also showed large differences not only in the variation pattern but also in magnitude (Figure S10). As discussed for the regional variations of the emission inventory (section 3.3), the MIX inventory showed similar seasonal variations to those of the REAS emission inventory, indicating high BC/CO ratios in winter for China (due to residential heating) and high values in summer for Japan (due to traffic). On the other hand, the seasonal variation of EDGAR reached the maximum in summer for China and in winter for South Korea and Japan, which is an opposite seasonal pattern to that of the REAS and MIX emission inventories. The reason why the summer ratio was high in China is that the emission rates from industry increased in summer. This tendency was prominent in North China due to the much higher BC/CO ratio (this was especially relevant for oil refineries and the transformation industry). High BC/CO ratios in winter in Korea and Japan were due to the reduced effect from road transportation, which has a low BC/CO ratio.” (L471-483)

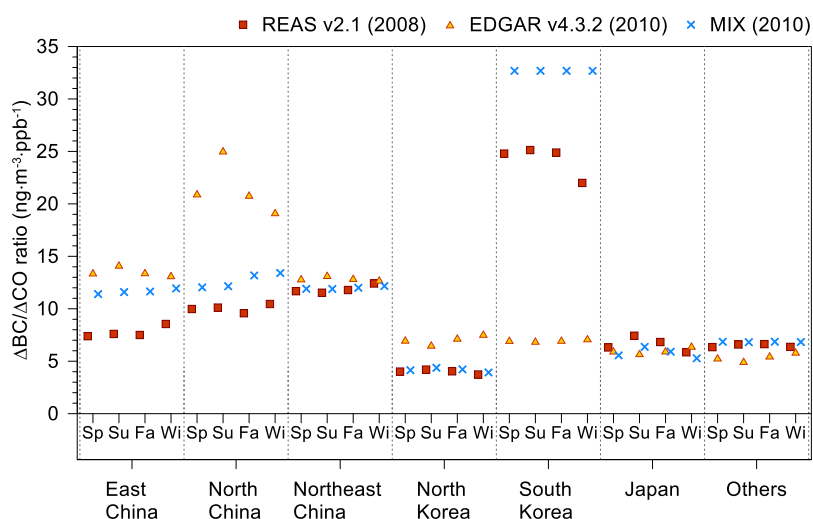


Figure S10. Seasonal variations of the overall regional mean BC/CO ratio according to different bottom-up emission inventories. The number in parentheses in each inventory indicates the base year. The abbreviation of ‘Sp’ to ‘Wi’ indicates spring to winter.

6. Have any of the measurements been affected by fires? Open biomass burning may change the BC/CO ratios substantially but is usually not well represented in emission inventories.

Because wild fire emissions are not included in the REAS inventory, we checked the influence of wild fire events with high BC/CO ratios by similar methods to recalculating REAS ratio using the Fire Information for Resource Management System (FIRMS) from the Moderate Resolution Imaging Spectroradiometer (MODIS). However, there was no significant difference between the results produced by including and excluding wild fire events at all sites (Welch’s t-test; $p > 0.1$), suggesting that the effect of wild fires could be

negligible when we accounted for the long-term variation.

We added relevant information as follows:

“In addition, we checked (1) the dry deposition effect during the traveling time ~~and~~, (2) the influences of other regions on $\Delta BC/\Delta CO$ depending on the residence time and (3) biomass burning events that could cause distortion producing higher $\Delta BC/\Delta CO$ values.” (L214-217)

“In addition, the influences from biomass burning were minimized during long-term periods, as confirmed by no significant difference between the ratios produced by including and excluding biomass burning events selected by the Moderate Resolution Imaging Spectroradiometer (MODIS) Fire Information for Resource Management System (FIRMS). Miyakawa et al. (2019) also pointed out that ~90% of BC in springtime at Fukue originated from the combustion of fossil fuel.” (L221-226)

Miyakawa, T., Komazaki, Y., Zhu, C., Taketani, F., Pan, X., Wang, Z., and Kanaya, Y.: Characterization of carbonaceous aerosols in Asian outflow in the spring of 2015: Importance of non-fossil fuel sources, *Atmos. Environ.*, 214, 116858, <https://doi.org/10.1016/j.atmosenv.2019.116858>, 2019.

1 **Regional variability in black carbon and carbon monoxide**
2 **ratio from long-term observations over East Asia:**
3 **Assessment of representativeness for BC and CO emission**
4 **inventories**

5
6 Yongjoo Choi^{1*}, Yugo Kanaya¹, Seung-Myung Park², Atsushi Matsuki³, Yasuhiro
7 Sadanaga⁴, Sang-Woo Kim⁵, Itsushi Uno⁶, Xiaole Pan⁷, Meehye Lee⁸, Hyunjae Kim², Dong
8 Hee Jung²

9
10 ¹ Research Institute for Global Change, Japan Agency for Marine-Earth Science and
11 Technology (JAMSTEC), Yokohama, 2360001, Japan

12 ² Division of Climate & Air Quality Research, National Institute of Environmental
13 Research, Kyungseo-dong, Seo-Gu, Incheon 404170, Korea

14 ³ Institute of Nature and Environmental Technology, Kanazawa University, Kanazawa
15 9201192, Japan

16 ⁴ Department of Applied Chemistry, Graduate School of Engineering, Osaka Prefecture
17 University, 1-1 Gakuen-cho, Naka-ku, Sakai, Osaka 5998531, Japan

18 ⁵ School of Earth and Environmental Sciences, Seoul National University, Seoul, Korea

19 ⁶ Research Institute for Applied Mechanics, Kyushu University, Kasuga Park 6-1,
20 Fukuoka, 816-8580, Japan

21 ⁷ Institute of Atmospheric Physics, Chinese Academy of Sciences, Beijing, China

22 ⁸ Department of Earth and Environmental Sciences, Korea University, Seoul, Korea

23
24 *Correspondence to: Yongjoo Choi (choingjoo@jamstec.go.jp)

25
26 Prepared for *Atmospheric Chemistry and Physics*

27 Revised in October 2019

28 **Abstract**

29 The black carbon (BC) and carbon monoxide (CO) emission ratios were estimated and
30 compiled from long-term, harmonized observations of the $\Delta BC/\Delta CO$ ratios under conditions
31 unaffected by wet deposition at four sites in East Asia, including two sites in Korea
32 (Baengnyeong and Gosan) and two sites in Japan (Noto and Fukuoka). Extended spatio-
33 temporal coverage enabled estimation of the full seasonality and elucidation of the emission
34 ratio in North Korea for the first time. The estimated ratios were used to validate the Regional
35 Emission inventory in ASia (REAS) version 2.1 based on six study domains (East China, North
36 China, Northeast China, South Korea, North Korea, and Japan). We found that the $\Delta BC/\Delta CO$
37 ratios from four sites converged into a narrow range ($6.2 - 7.9 \text{ ng m}^{-3} \text{ ppb}^{-1}$), suggesting
38 consistency in the results from independent observations and similarity in source profiles over
39 the regions. The BC/CO ratios from the REAS emission inventory ($7.7 \text{ ng m}^{-3} \text{ ppb}^{-1}$ for East
40 China – $23.2 \text{ ng m}^{-3} \text{ ppb}^{-1}$ for South Korea) were overestimated by factors of 1.1 for East China
41 to 3.0 for South Korea, whereas the ratio for North Korea ($3.7 \text{ ng m}^{-3} \text{ ppb}^{-1}$ from REAS) was
42 underestimated by a factor of 2.0, most likely due to inaccurate emissions from the road
43 transportation sector. Seasonal variation in the BC/CO ratio from REAS was found to be the
44 highest in winter (China and North Korea) or summer (South Korea and Japan), whereas the
45 measured $\Delta BC/\Delta CO$ ratio was the highest in spring in all source regions, indicating the need
46 for further characterization of the seasonality when creating a bottom-up emission inventory.
47 At levels of administrative districts, overestimation in Seoul, the southwestern regions of South
48 Korea, and Northeast China was noticeable, and underestimation was mainly observed in the
49 western regions in North Korea, including Pyongyang. These diagnoses are useful for
50 identifying regions where revisions in the inventory are necessary, providing guidance for the
51 refinement of BC and CO emission rate estimates over East Asia.

52 **1 Introduction**

53 Black carbon (BC), emitted from the incomplete combustion of fossil fuel and/or biomass
54 burning, absorbs solar radiation and reduces the surface albedo of snow/ice after dry/wet
55 deposition (Samset, 2018; Bond et al., 2013); thereby augmenting the global warming trend
56 primarily induced by increased levels of carbon dioxide (CO₂) (Ramanathan and Carmichael,
57 2008; Jacobson, 2001; Myhre et al., 2013). In addition to global warming effects, BC is
58 significantly associated with cardiovascular mortality (Smith et al., 2009; Geng et al., 2013),
59 and is more related to health effects than PM_{2.5} (particulate matter having an aerodynamic
60 diameter $\leq 2.5 \mu\text{m}$) (Janssen et al., 2011, 2012; Loomis et al., 2013).

61 In particular, the BC emissions from China, which accounted for 31% of the total annual
62 global emissions in 2012 (Crippa et al., 2018), showed an increasing trend from 1970 to 2012
63 (Kurokawa et al., 2013; Ohara et al., 2007; Crippa et al., 2018). To enhance the understanding
64 of the behavior of BC in the atmosphere, it is essential to obtain a reliable BC concentration
65 along with model simulations based on accurate bottom-up emission inventories. The bottom-
66 up emission inventories may be subject to large uncertainties associated with emission factors
67 from various types of combustion sources, countries and species (Kurokawa et al., 2013),
68 although the uncertainty in BC emissions decreased from 160.2% in 1970 to 74.3% in 2012
69 (Crippa et al., 2018). BC and carbon monoxide (CO) are byproducts of the incomplete
70 combustion of carbon-based fuels, and the ratio between ΔBC (the difference from the baseline
71 level) and ΔCO could be a useful parameter for characterizing combustion types. Using these
72 characteristics, past studies used the $\Delta\text{BC}/\Delta\text{CO}$ ratio to identify emission source types (Guo et
73 al., 2017; Pan et al., 2011; 2013; Zhu et al., 2019) and/or validate BC emissions from bottom-
74 up inventories (Han et al., 2009; Wang et al., 2011; Verma et al., 2011; Sahu et al., 2009; Kondo
75 et al., 2006). However, it was hard to diagnose the accuracy of emission inventories over East
76 Asia from those studies because either data covering short, intensive measurement periods at a
77 single site were used or the studied source regions did not necessarily match the administrative
78 districts for which a detailed emission inventory was constructed. In addition, BC
79 concentrations can differ depending on the instruments and operation protocols used for
80 observations—such discordance yet poses a major obstacle to obtaining a comprehensive
81 understanding. Kondo (2015) compiled $\Delta\text{BC}/\Delta\text{CO}$ ratios from systematic observations in Asia.
82 However, information during the 2010s, when emissions patterns changed significantly, has

83 not been covered. Kanaya et al. (2016) used observations at Fukue Island for 6 years (2009-
84 2015) to derive a region-specific $\Delta\text{BC}/\Delta\text{CO}$ emission ratio. However, the seasons were limited
85 to autumn-spring, and the footprint over each source region was still limited, as observations
86 at a single site were analyzed.

87 In this study, we investigated the $\Delta\text{BC}/\Delta\text{CO}$ ratios from long-term measurements at four
88 measurement sites (two Korean and two Japanese sites which were measured for more than a
89 year) over East Asia in order to comprehensively evaluate the Regional Emission inventory in
90 ASia (REAS) [version 2.1 based on the 2008](#) emission inventory (Kurokawa et al., 2013) of BC
91 and CO with sufficient spatio-temporal coverage. [The REAS inventory comprises emissions](#)
92 [data from 30 Asian countries and regions, including China, North Korea, South Korea and](#)
93 [Japan, between the years 2000 and 2008 at a \$0.25^\circ \times 0.25^\circ\$ horizontal resolution. The emissions](#)
94 [sources consisted of power plants, combustible and non-combustible sources in industry, on-](#)
95 [road and off-road sources in transport, and residential and other activities, such as agricultural](#)
96 [activities and evaporative sources \(Han et al., 2015; Itahashi et al., 2017; Kurokawa et al., 2013;](#)
97 [Saikawa et al., 2017; Uno et al., 2017\).](#) The improved spatio-temporal coverage enabled
98 estimation of the full seasonality and elucidation of the emissions ratio from North Korea for
99 the first time. By comparing the regional and seasonal $\Delta\text{BC}/\Delta\text{CO}$ ratios between the REAS
100 emission inventory and the measurements, this study identifies the points of improvement for
101 bottom-up emission inventories.

102

103 **2 Methodology**

104 **2.1 Measurement sites and periods**

105 Figure 1 shows the locations of the measurement sites in this study. Both Baengnyeong
106 (124.63°E , 37.97°N) and Gosan (126.17°E , 33.28°N) are representative background sites in
107 Korea. The Baengnyeong site is an intensive measurement station operated by the Korean
108 Ministry of Environment. The Gosan site is a supersite of many international campaigns, such
109 as Aerosol Characterization Experiments (ACE)-Asia (Huebert et al., 2003), Atmospheric
110 Brown Cloud (ABC) (Nakajima et al., 2007) and Cheju ABC Plume–Monsoon Experiment
111 (CAPMEX) (Ramana et al., 2010). Since the two sites in Korea are located in the western
112 region of the Korean peninsula with similar longitudes but different latitudes, these sites are

113 suitable for monitoring pollutant transport from China, North Korea (especially Baengnyeong)
114 and South Korea. In Japan, the Fukuoka site (33.52 °N, 130.47 °E) is located at the Chikushi
115 Campus of Kyushu University located in the suburbs of Fukuoka, and the site is the largest
116 center of commerce on the island of Kyushu (Itahashi et al., 2017; Uno et al., 2017). The Noto
117 site (37.45 °N, 137.36 °E) is located at the Ground-based Research Observatory (NOTOGRO),
118 which has been apart from Kanazawa and Toyama, the nearest provincial cities, by
119 approximately 115 km southwest and 85 km south, respectively. Therefore, Noto is a suitable
120 place for monitoring the background concentrations and/or outflows of pollution from the
121 Asian continent (Ueda et al., 2016). The measurement periods were commonly in the early
122 2010s, while slight differences were present among the sites (Table 1). The longest
123 measurement period was in Noto for approximately six years (from 2011 to 2016), followed
124 by those in Baengnyeong (five years), Gosan (three years), and Fukuoka (one and a half years).
125 The measurements in Baengnyeong did not include 2011 to 2012 due to the absence of CO
126 data.

127

128 **2.2 Instruments**

129 It is crucial to ensure reliable atmospheric BC concentrations, which were measured by
130 different instruments, by excluding the effects of co-existing scattering particles. To keep the
131 harmonization, we considered BC concentrations to be reliable when the data were measured
132 by pre-validated instruments reported to have good agreement between instruments, including
133 OC-EC analyzers (Sunset Laboratory Inc., USA) with optical corrections, [single-particle soot](#)
134 [photometers \(SP2\)](#), continuous soot-monitoring systems (COSMOS) and multi-angle
135 absorption photometers (MAAP 5012 Thermo Scientific) (e.g., [Kondo et al., 2011](#); Kanaya et
136 al., [2008](#), 2013, [2016](#); [Miyakawa et al., 2016, 2017](#); [Taketani et al., 2016](#); [Ohata et al., 2019](#)).

137 Hourly elemental carbon (EC) concentrations in PM_{2.5} at the Baengnyeong site were
138 measured by a model-4 semi-continuous OC-EC field analyzer using the thermal/optical
139 transmittance (TOT) method and the non-dispersive infrared (NDIR) method based on NIOSH
140 method 5040 (NIOSH, 1996). The particles passed through a PM_{2.5} cyclone with 8.0 L/min and
141 a carbon impregnated multi-channel parallel plate diffusion denuder (Turpin et al., 2000), and
142 were collected on a quartz fiber filter during 45 min. OC and EC were then analyzed during
143 the last 15 min. The detection limit of EC, which is defined as twice the average of the field

144 blanks, was reported to be 30 ng m^{-3} , and the precision of EC was 7.5% (Park et al., 2013).

145 At both Noto and Fukuoka sites, $\text{PM}_{2.5}$ BC concentrations were measured using a MAAP.
146 The BC concentration is converted from the absorption coefficients, which were determined
147 by measuring both the transmittance and reflectance of a filter loaded with aerosols. Because
148 the MAAP installed a light detector that locates light reflected from the filter at 130° and 165°
149 from the illumination direction (Petzold et al., 2005), the MAAP can correct for scattering
150 particle effects. It should be noted that we used a different mass absorption efficiency (MAE)
151 value of $10.3 \text{ m}^2 \text{ g}^{-1}$, as suggested by Kanaya et al. (2013), instead of the default MAE of 6.6
152 $\text{m}^2 \text{ g}^{-1}$, ~~which showed perfect correlation with the COSMOS BC concentration (Kanaya et al.,~~
153 ~~2013).~~ This value was validated with COSMOS, which showed a reliable performance with
154 SP2 and OC-EC analyzer (Miyakawa et al., 2017; Kondo et al., 2011; Ohata et al., 2019) on a
155 long-term basis at Fukue (Kanaya et al., 2016) and in Tokyo (Kanaya et al., 2013). The
156 consistency between MAAP and SP2 at Noto was reported at $\sim 10\%$ (Taketani et al., 2016). At
157 Fukuoka, a similar behavior was expected as the BC there would be a mixture from the
158 continent and urban sources, as experienced at Fukue and Tokyo. The reported minimum
159 detection limit of the MAAP was different depending on the averaging time as 12 ng m^{-3} for
160 one hour and 64 ng m^{-3} for one minute by applying the revised MAE ($10.3 \text{ m}^2 \text{ g}^{-1}$).

161 The Gosan site has monitored BC concentrations using a continuous light absorption
162 photometer (CLAP) with three wavelengths including 467, 528, and 652 nm (Cho et al., 2019).
163 Through PM_1 and PM_{10} impactors, which were switched every 30 min, the particles were
164 collected on 47-mm diameter glass-fiber filters (Pallflex type E70-2075W). The volumetric
165 flow rate was 1 L/min. The raw absorption coefficient of the CLAP was corrected using the
166 methods of Bond et al. (1999) to eliminate effects due to filter loading errors. The absorption
167 coefficient at 528 nm was used to determine the BC concentration by applying $10 \text{ m}^2 \text{ g}^{-1}$ for
168 MAE. In this study, we used the PM_1 BC concentration because BC particles mainly exist in
169 less than $1 \mu\text{m}$ (Miyakawa et al., 2017; Bond et al., 2013). Although the uncertainty derived
170 from scattering particles was reported to be $\sim 25\%$ at Gosan (Ogren et al., 2017), the BC from
171 CLAP was verified by comparison with a co-located semi-continuous OC-EC field analyzer
172 (Lim et al., 2012). The slope of the best fit line through the origin was close to one as 1.17,
173 implying that the PM_1 BC concentration from CLAP was well consistent with that from $\text{PM}_{2.5}$
174 EC.

175 Hourly CO concentrations were measured by a gas filter correlation CO analyzer (Model
176 300EU, Teledyne-API Inc.) at Baengnyeong and nondispersive infrared absorption
177 photometers (48C, Thermo Scientific) at the other three sites. The overall uncertainties of the
178 BC and CO measurements were estimated to be less than 15% (except for Gosan, at 20%) and
179 5%, respectively. The overall regional $\Delta BC/\Delta CO$ ratio varied from -0.7 (-8%) to 0.8 (10%) due
180 to uncertainty.

181

182 2.3 $\Delta BC/\Delta CO$ ratio and allocation of the dominant emission region

183 To identify the origin of BC and CO emission sources, backward trajectories at 500 m during
184 the past five days (120 hours) were calculated by the Hybrid Single Particle Lagrangian
185 Integrated Trajectory (HYSPLIT) 4 model (Draxler et al., 2018) for every six hour interval (00,
186 06, 12 and 18 UTC) using the Global Data Assimilation System (GDAS) with a horizontal
187 resolution of $1^\circ \times 1^\circ$, as the GDAS with 0.5° resolution did not account for vertical motion (Su
188 et al., 2015). The spatial distribution of the number of endpoints for backward trajectories from
189 the four measurement sites revealed the large spatial coverage of the footprint over East Asia
190 (Figure S1). These four sites could be representative for monitoring outflows from China and
191 Korea because of the dominance of wintertime monsoons. Moreover, the footprint of the Noto
192 site could cover the middle part of Japan, such as the Kanto, Chubu, and Kansai regions. To
193 exclude cases with wet deposition influence, the accumulated precipitation along with
194 trajectory (APT) was calculated over the past 72 hours (Kanaya et al., 2016; Oshima et al.,
195 2012), and we only used cases with $APT = 0$.

196 As aforementioned, BC and CO are commonly emitted from incomplete fuel combustion,
197 and the $\Delta BC/\Delta CO$ ratio is used to evaluate the bottom-up emission inventory as a
198 representative indicator, preserving the emission ratio when wet removal is not influential
199 (Kanaya et al., 2016). ΔCO was calculated by subtracting the baseline level (~~determined as a~~
200 ~~14-day moving 5th percentile~~) from the observed CO mixing ratio. Though there are several
201 methods for estimating the CO baseline level (e.g., Matsui et al., 2011; Miyakawa et al. 2017;
202 Oshima et al., 2012; Verma et al. 2011), the CO baseline in this study was regarded as a 14-day
203 moving 5th percentile based on Kanaya et al. (2016). On the other hand, ΔBC is the BC
204 concentration as is (BC baseline = 0), because the ~~baseline concentration~~ atmospheric lifetime

205 of BC ~~was assumed~~ is estimated to be ~~zero~~ several days (Park et al., 2005), in contrast to that
206 of CO, which has a one- or two-month lifetime (Bey et al. 2001). It should be noted that we
207 used the CO concentration when it was higher than the moving 25th percentile of CO, so that
208 only data with meaningful enhancement was employed.

209 To determine the dominant emission region of each sample, we calculated the residence time
210 over the six regions (East China, North China, Northeast China, North Korea, South Korea,
211 and Japan) using backward trajectories covering the previous 72 hours. Hourly endpoints with
212 altitudes of less than 2.5 km were counted (Kanaya et al., 2016). Based on the fractions of the
213 total 73 hours, the highest fraction of the region was classified as the dominant emission region
214 when the fraction of the frequency was higher than 5% to secure statistics (S1; Figure S2). In
215 addition, we checked (1) the dry deposition effect during the traveling time ~~and~~, (2) the
216 influences of other regions on $\Delta BC/\Delta CO$ depending on the residence time ~~and~~ (3) biomass
217 burning events that could cause distortion producing higher $\Delta BC/\Delta CO$ values. As a result, it
218 was determined that there was no significant dry deposition effect (S2; Figure S3) or interrupted
219 by other regions (S3; Figure S4), implying that the BC/CO ratio was preserved regardless of
220 the residence time over other regions when the threshold ($N > 5$) of each bin (20% interval)
221 was satisfied. In addition, the influences from biomass burning were minimized during long-
222 term periods, as confirmed by no significant difference between the ratios produced by
223 including and excluding biomass burning events selected by the Moderate Resolution Imaging
224 Spectroradiometer (MODIS) Fire Information for Resource Management System (FIRMS).
225 Miyakawa et al. (2019) also pointed out that ~90% of BC in springtime at Fukue originated
226 from the combustion of fossil fuel.

227 The uncertainty of the BC/CO ratio that may arise from estimating the CO baseline by
228 different methods and from allocation methods involving selecting different altitudes are
229 discussed in the Supplement (S4).

231 **3 Results and discussion**

232 **3.1 Seasonal variation in BC and CO**

233 The BC, CO, and ΔCO concentrations are summarized in Table 2. The mean BC and ΔCO
234 concentrations were highest in Baengnyeong, followed by Fukuoka, Gosan, and Noto,

235 according to the distance from the main BC and CO emission sources, China. Although the
236 levels at Baengnyeong and Gosan were high, they maintained regional representativeness, as
237 the BC concentration levels were lower than those at urban sites such as Daejeon ($1.78 \mu\text{g m}^{-3}$),
238 Seoul ($1.52 \mu\text{g m}^{-3}$), and Gwangju ($1.13 \mu\text{g m}^{-3}$) in Korea (Yu et al., 2018). Despite the
239 suburban location of Fukuoka, the BC ~~and ΔCO concentrations were~~ concentration was even
240 lower than ~~those that~~ of Baengnyeong. However, the CO baseline concentration was highest
241 among the measurement sites suggesting the influence of local sources, though it could be
242 varied depending on geographical location. To check influence of local pollution at Fukuoka,
243 we tested by applying more stringent CO baseline criteria (14-days moving 2 % percentile;
244 ~ 166 ppbv). As a result, there was no significant changes in our results (less than -4 %).
245 ~~indicating that the measurement site could not be seriously influenced by local sources.~~ In the
246 case of Noto, the BC concentration was the lowest among the sites as $0.24 \mu\text{g m}^{-3}$. The
247 concentration level was lower than the annual averages of $0.36 \mu\text{g m}^{-3}$ at Fukue (Kanaya et al.,
248 2016) and $0.29 \mu\text{g m}^{-3}$ at Cape Hedo (Verma et al., 2011), which are regarded as background
249 monitoring sites in Japan. The seasonal variation in the BC concentration at all sites showed
250 similar patterns of being low in summer due to rainout followed by precipitation and increasing
251 from fall due to house heating and/or crop biomass burning, along with the transition to
252 westerly winds.

253 Figure 2 shows the time series of the BC, CO, $\Delta\text{BC}/\Delta\text{CO}$ ratio and APTs at the Noto site.
254 Regardless of precipitation during the measurement periods, the correlation coefficient (R)
255 between BC and CO was 0.70 within the significance level ($p < 0.01$), indicating that BC and
256 CO were emitted from similar sources. Additionally, the R between $\Delta\text{BC}/\Delta\text{CO}$ and APT
257 showed a slightly negative relationship as -0.24 within the significance level ($p < 0.01$),
258 suggesting that the wet removal process removed BC, which resulted in a low $\Delta\text{BC}/\Delta\text{CO}$ ratio.
259 However, compared to Noto, the other sites showed weak negative relationships within the
260 significance level ($p < 0.01$) because the amounts of APT at the other three sites were lower
261 than that for Noto, which led to less distinctive wet removal effects (Table 2).

262

263 3.2 Regional variation in the $\Delta\text{BC}/\Delta\text{CO}$ ratio

264 Figure 3 shows a comparison of the $\Delta\text{BC}/\Delta\text{CO}$ ratio between the REAS emission inventories

265 and measured values at four sites. The solid symbols with error bars satisfy the fraction of
266 frequency ($> 5\%$ in Figure S2) and the number of data for each bin ($N > 5$ in Figure S4). The
267 open symbols with a dashed error bar were excluded from the analysis because they did not
268 satisfy the criteria. It should be noted that the total number of data for dominant emission
269 regions in this study was 2.7 times higher than that used by Kanaya et al. (2016), indicating
270 significant improvement in the representativeness of the regional variation. Due to the large
271 spatial variations in BC and CO in the REAS emission inventory depending on the dominant
272 emission region, the coefficient of variation (CV; standard deviation divided by the mean) of
273 the BC/CO ratio from the REAS emission inventory (0.65, over the six regions) was much
274 higher than those from the measurements (0.09 – 0.13) at each site. The CV from the REAS
275 emission inventory was still as high as 0.27 when the highest (South Korea) and the lowest
276 ratios (North Korea) were excluded. Moreover, the BC/CO ratio from the REAS emission
277 inventory was slightly higher than the measured ratios, except for North Korea, indicating that
278 the REAS BC/CO ratio did not represent the real value. It should be noted that there were no
279 significant changes in trends for the long-term variation of the $\Delta BC/\Delta CO$ ratios of all sites, as
280 well as BC/CO ratios from the Emissions Database for Global Atmospheric Research (EDGAR
281 version 4.3.2; Crippa et al. 2018) emission inventory since 2008 and the MIX emission
282 inventory (Li et al., 2017) in 2008 and 2010 (Figure S6). This result implied that comparison
283 between the measurements and the REAS emission inventory was a reasonable approach, even
284 though the time scale between them did not match. The differences in the ratios between the
285 REAS and the measurements will be discussed further in section 3.3.

286 The $\Delta BC/\Delta CO$ ratio in North China showed the lowest average value across China as $6.2 \pm$
287 $0.5 \text{ ng m}^{-3} \text{ ppb}^{-1}$, followed by East China ($6.8 \pm 0.3 \text{ ng m}^{-3} \text{ ppb}^{-1}$) and Northeast China ($7.9 \pm$
288 $0.7 \text{ ng m}^{-3} \text{ ppb}^{-1}$). The ratios of two or three regions in China showed significant differences
289 at all sites when Welch's t-test or the ANOVA test was applied ($p < 0.05$), except for
290 Baengnyeong. The lower $\Delta BC/\Delta CO$ ratio in North China than in East China was also reported
291 with 5.3 ± 2.1 and $6.4 \pm 2.2 \text{ ng m}^{-3} \text{ ppb}^{-1}$ in Fukue, 7.0 ± 3.3 and $7.5 \pm 4.6 \text{ ng m}^{-3} \text{ ppb}^{-1}$ in
292 Cape Hedo, and 6.5 ± 0.4 and $8.8 \pm 0.9 \text{ ng m}^{-3} \text{ ppb}^{-1}$ in Mt. Huang, respectively (Kanaya et al.,
293 2016; Pan et al., 2011; Verma et al., 2011). In the case of Northeast China, the variation in the
294 ratio over the measurement sites (0.09 of CV) was higher than that over other Chinese regions
295 (0.07 and 0.04 of CV in East China and North China, respectively). The reason why a higher
296 CV was observed even in the same emission source region is that the pathways of the backward

trajectories were different, depending on the measurement site (Figure S5S7); the backward trajectory of Noto passed over the eastern region (Heilongjiang), whereas that of Baengnyeong passed over the western region of Northeast China (Liaoning). The information of Northeast China emissions obtained from measurements at Gosan might have been more strongly affected by emissions from South Korea than that at Baengnyeong (S4S5).

The mean $\Delta BC/\Delta CO$ ratios of North Korea and South Korea were similar as 7.3 and $7.8 \pm 1.2 \text{ ng m}^{-3} \text{ ppb}^{-1}$, respectively. Verma et al. (2011) reported a lower ratio for the Korean peninsula (both South and North Korea) as $5.7 \pm 2.0 \text{ ng m}^{-3} \text{ ppb}^{-1}$. It should be noted that the $\Delta BC/\Delta CO$ ratios for South Korea estimated from observations at Korean and Japanese sites were significantly different as $8.9 \pm 5.3 \text{ ng m}^{-3} \text{ ppb}^{-1}$ and $6.7 \pm 3.8 \text{ ng m}^{-3} \text{ ppb}^{-1}$, respectively ($p \leq 0.01$). These differences were also consistent with previous studies that reported ratios as $8.5 \text{ ng m}^{-3} \text{ ppb}^{-1}$ at Gosan (Sahu et al., 2009) and $6.7 \pm 3.7 \text{ ng m}^{-3} \text{ ppb}^{-1}$ at Fukue (Kanaya et al., 2016). This difference between the ratios could also be caused by the different influences of the emission source regions, similar to the case in Northeast China. Baengnyeong and Gosan were mainly influenced by the southwestern region of Korea, including the Seoul Metropolitan Area (SMA), whereas the Fukuoka and Noto sites were mainly influenced by the southeastern region of Korea (Figure S6S8), suggesting large spatial variation in BC/CO over the Korean peninsula. In the case of Japan, the mean $\Delta BC/\Delta CO$ ratio was $6.8 \pm 0.2 \text{ ng m}^{-3} \text{ ppb}^{-1}$, which was higher than or similar to the reported values as $5.9 \pm 3.4 \text{ ng m}^{-3} \text{ ppb}^{-1}$ at Fukue, $5.7 \pm 0.9 \text{ ng m}^{-3} \text{ ppb}^{-1}$ at Tokyo and $6.3 \pm 0.5 \text{ ng m}^{-3} \text{ ppb}^{-1}$ at Nagoya (Kondo et al., 2006; Kanaya et al., 2016). Moreover, there were no significant differences in the $\Delta BC/\Delta CO$ ratio between Noto and Fukuoka, although the trajectories passed through different regions of Japan (Figure S7S9), suggesting that the spatial variation in the $\Delta BC/\Delta CO$ ratio of Japan was smaller than that of South Korea. The higher $\Delta BC/\Delta CO$ ratio of South Korea could be explained by the higher ratio of diesel to gasoline vehicles in Korea (0.88) than in Japan (0.09) in 2015 (MLIT 2019; MOLIT 2019) because the BC/CO ratio from diesel vehicles is higher than that from gasoline vehicles due to the different carbon atom contents (Zhou et al., 2009; Guo et al., 2017).

3.3 Comparison between the REAS v2.1 and measured $\Delta BC/\Delta CO$ ratios

In this section, we investigated the differences in $\Delta BC/\Delta CO$ between the measured values

327 and the REAS v2.1 emission inventory. We adopted the mean fractional bias (MFB, ranging
328 from -2 to 2) defined by

$$329 \quad \text{MFB} = \frac{2}{N} \sum_{i=1}^{i=N} \frac{R_i - M_i}{R_i + M_i} \quad (1)$$

330 where R_i and M_i denote the REAS emission inventory and the measured ratio corresponding to
331 sample i , respectively.

332 East China showed the lowest MFB value among Chinese regions as 0.12, and the other two
333 regions had similar MFB values as 0.48 for North China and 0.35 for Northeast China,
334 indicating an overestimation of the REAS emission inventory in China. The BC/CO ratio from
335 the REAS emission inventory showed a higher ratio in North China ($10.0 \text{ ng m}^{-3} \text{ ppb}^{-1}$) than
336 in East China ($7.7 \text{ ng m}^{-3} \text{ ppb}^{-1}$), which is an opposite pattern to that of the measured ratios.
337 Considering that most trajectories passed Nei Mongol ($12.5 \text{ ng m}^{-3} \text{ ppb}^{-1}$) and Hebei (6.6 ng
338 $\text{m}^{-3} \text{ ppb}^{-1}$) in North China with a lower measured $\Delta\text{BC}/\Delta\text{CO}$ ratios, the BC/CO ratio in Nei
339 Mongol was likely overestimated. In Northeast China, the higher BC/CO ratio in Heilongjiang
340 ($14.0 \text{ ng m}^{-3} \text{ ppb}^{-1}$ in REAS) than in Liaoning ($11.3 \text{ ng m}^{-3} \text{ ppb}^{-1}$ in REAS) was consistent
341 with the tendency of the measured $\Delta\text{BC}/\Delta\text{CO}$ ratio.

342 The BC/CO ratios from the REAS emission inventory for South Korea ($23.2 \text{ ng m}^{-3} \text{ ppb}^{-1}$)
343 and North Korea ($3.7 \text{ ng m}^{-3} \text{ ppb}^{-1}$) were highly over- and underestimated, along with large
344 absolute values of MFB of 0.99 (by factor 3.0) and -0.66 (by factor 2.0), respectively. The
345 $\Delta\text{BC}/\Delta\text{CO}$ ratio in South Korea was still found to be $9.6 \pm 0.5 \text{ ng m}^{-3} \text{ ppb}^{-1}$ when the condition
346 was restricted to less than the 25th percentile of the maximum relative humidity during the
347 previous 72 hours (less than 67.2%) to ensure choosing cases without wet deposition effects.
348 Kanaya et al. (2016) pointed out that the industry and transport sectors could be the sources of
349 the large discrepancy between the REAS emission inventory and the measurements. Although
350 the ratio of the industry sector in South Korea ($41.4 \text{ ng m}^{-3} \text{ ppb}^{-1}$) is also much higher (13
351 times) than that in Japan, BC and CO from industrial emissions in South Korea only accounted
352 for 13.4% and 7.9% of the total, respectively. Here, we identify the relative importance of the
353 road transport sector; the BC/CO ratio from road transportation in South Korea was 26.8 ng
354 $\text{m}^{-3} \text{ ppb}^{-1}$, which was 3.6 times higher than the ratio in Japan as $7.4 \text{ ng m}^{-3} \text{ ppb}^{-1}$. Upon looking
355 more closely into the transportation sector, the BC/CO ratios from diesel vehicles were found

356 to be similar between S. Korea ($120 \text{ ng m}^{-3} \text{ ppb}^{-1}$) and Japan ($109 \text{ ng m}^{-3} \text{ ppb}^{-1}$), although the
357 BC emissions could vary depending on the installation of diesel particulate filters.

358 To easily compare the CO emission rates from gasoline vehicles between South Korea and
359 Japan, we roughly estimated the CO emission factor from gasoline vehicles. This hypothetical
360 CO emission factor was calculated by considering the actual mean daily mileages (31 and 12
361 km day^{-1} for South Korea and Japan, respectively), the actual number of gasoline vehicles in
362 2008 (MLIT 2016, 2019; MOLIT 2019; TS, 2009) and the total CO emission rates in the REAS
363 emission inventory; the hypothetical CO emission factor in Japan ($15.8 \text{ CO g km}^{-1}$; 2.82 Tg yr^{-1}
364 from 40.8 million) was 6.9 times higher than that in Korea (2.3 CO g km^{-1} ; 0.22 Tg yr^{-1}
365 from 8.3 million). Underestimation of the hypothetical CO emission factor in South Korea was
366 also observed in motorcycles (2.8 CO g km^{-1} ; 0.06 Tg yr^{-1} from 1.8 million), which was lower
367 than that in Japan (14.7 g km^{-1} ; 0.15 Tg yr^{-1} from 1.5 million), assuming the same motorcycle
368 mileages in South Korea. Clearly the hypothetical CO emission factor thus derived for Korea
369 is unlikely, pointing to underestimation of the assumed CO emission rate. We can roughly
370 revise the total CO emission rates (2.2 Tg) from gasoline vehicles (1.46 Tg) and motorcycles
371 (0.31 Tg) by applying the hypothetical CO emission factor of Japan. Although the hypothetical
372 CO emission factors had large uncertainties due to inaccurate mileages for gasoline vehicles
373 and motorcycles, the revised REAS BC/CO ratio decreased to $7.3 \text{ ng m}^{-3} \text{ ppb}^{-1}$, which was
374 closer to that of the observations.

375 The recently updated Korean emission inventory Clean Air Policy Support System (CAPSS;
376 Lee et al. 2012; Yeo et al., 2019) based on 2015 also showed a high BC/CO ratio as 25.1 ng
377 $\text{m}^{-3} \text{ ppb}^{-1}$ (Table 3), with much lower hypothetical CO emission factors for gasoline vehicles
378 (1.1 CO g km^{-1}) and motorcycles (1.7 CO g km^{-1}) with similar mean mileage values (30.4 km
379 day^{-1} ; TS, 2015), suggesting that BC and CO emissions still need to be improved. This high
380 BC/CO ratio ($35.6 \text{ ng m}^{-3} \text{ ppb}^{-1}$) was also found in the MIX emission inventory, whereas the
381 BC/CO ratio from the EDGAR inventory in 2010 was much closer to the measured ratio as
382 $7.68 \text{ ng m}^{-3} \text{ ppb}^{-1}$. Many researchers have been trying to improve the accuracy of the CO
383 emission rate in South Korea through the bottom-up emission inventory (0.90 Tg) and top-
384 down estimation (1.10 Tg) derived from the KORUS-AQ campaign (Table 3). However,
385 discrepancies still exist in not only the $\Delta\text{BC}/\Delta\text{CO}$ ratio but also the CO emission rate. In
386 particular, the CO emission rate in South Korea showed large variations according to the

387 emission inventory, suggesting that CO emission rates over South Korea should be improved
388 preferentially.

389 In the case of North Korea, the CO emission rate (5.14 Tg) from REAS was considerably
390 higher than that of South Korea by a factor of 7.4 and was especially higher than that of Japan,
391 resulting in a low BC/CO ratio as $3.7 \text{ ng m}^{-3} \text{ ppb}^{-1}$. The domestic and industrial sectors in
392 North Korea showed relatively low BC/CO ratios as 6.79 and $4.45 \text{ ng m}^{-3} \text{ ppb}^{-1}$, respectively,
393 compared to those in China ($9.5 - 10.5 \text{ ng m}^{-3} \text{ ppb}^{-1}$ for industry and $13.9 - 15.6 \text{ ng m}^{-3} \text{ ppb}^{-1}$
394 for the domestic sector). The BC and CO emission rates were under- and/or overestimated,
395 respectively, although the quality of fuel and/or end-of-pipe technology could be different. In
396 addition, when we considered registered vehicles in North Korea (0.26 million) and South
397 Korea (16.8 million), the CO emission from road transportation in North Korea (1.75 Tg) was
398 similar to the roughly revised CO emission in South Korea (1.88 Tg), implying a highly
399 overestimated CO emission rate for the transportation sector (Statics of Korea, 2017). The
400 Comprehensive Regional Emissions inventory for Atmospheric Transport Experiment
401 (CREATE; Woo et al., 2014) in 2015 and EDGAR reported much lower CO emission rates in
402 North Korea (1.41 and 1.55 Tg, respectively). As a result, the BC/CO ratio from EDGAR falls
403 within a reasonable range as $6.85 \text{ ng m}^{-3} \text{ ppb}^{-1}$, indicating agreement with the measured ratio
404 ($7.3 \text{ ng m}^{-3} \text{ ppb}^{-1}$). This is because the ratio in EDGAR CO emission rates relative to REAS
405 rates (30% of REAS) was much smaller than that for EDGAR BC (56% of REAS; Table 3),
406 especially in the road transportation (9% for CO and 21% for BC) and industry sectors (38%
407 for CO and 51% for BC). Kim and Kim (2019) pointed out that the uncertainty in the REAS
408 CO emission rate in North Korea could result from inaccurate emission factors for biofuel
409 compared to fossil fuels because the REAS emission inventory included several biofuel sources
410 (such as fuel wood, crop residue, and animal waste).

411 The mean $\Delta\text{BC}/\Delta\text{CO}$ ratio in Japan showed good consistency between the REAS emission
412 inventory ($6.84 \text{ ng m}^{-3} \text{ ppb}^{-1}$), along with lowest absolute MFB as -0.05, which was close to
413 0.09 from Kanaya et al. (2016). The BC and CO emission rates from EDGAR, MIX and
414 ECLIPSE V5a were close to those from the REAS emission inventory, indicating that the BC
415 and CO emission rates over Japan were more accurate than those over other regions (Table 3).

416 In the case of the MIX emission inventory, the emission rates from North and South Korea
417 were derived from the REAS and CAPSS inventories, respectively, and both the emission rates

418 and BC/CO ratio were within a narrow range of those of the REAS inventory. However, for
419 EDGAR, while the BC/CO ratios in North Korea, South Korea, and Japan were relatively
420 consistent with the ratios from measurements, the overestimation for China was remarkable
421 compared to both the measurement ratios and other emission inventories. Especially, North
422 China showed the highest BC/CO ratio compared to East and Northeast China, because the
423 industry sector in North China has the largest BC and CO emission rates (63% and 35% of
424 total, respectively), along with a high BC/CO ratio ($38.5 \text{ ng m}^{-3} \text{ ppb}^{-1}$).

425

426 **3.4 Seasonal variation in the $\Delta\text{BC}/\Delta\text{CO}$ ratio**

427 The regional $\Delta\text{BC}/\Delta\text{CO}$ ratios in the previous sections might still contain variability because
428 of spatial (differences in the pathways of trajectories) and/or temporal variation (differences in
429 monthly emissions), even within the same dominant emission region. To explore this finer
430 spatio-temporal variability in the $\Delta\text{BC}/\Delta\text{CO}$ ratio, the monthly BC and CO emission rates in
431 each grid (0.25° by 0.25°) in the REAS emission inventory were integrated over the pathway
432 of the backward trajectory satisfying altitudes ≤ 2.5 km and were compared with the
433 observations. Figure 4 shows the seasonal variation in the recalculated BC/CO ratios from the
434 REAS emission inventory and the measured $\Delta\text{BC}/\Delta\text{CO}$ ratios, regardless of the measurement
435 sites.

436 The recalculated BC/CO ratios of China and North Korea showed similar seasonal variations,
437 relatively high in winter and low in summer. This result was caused by the seasonal variation
438 in the BC emission rate (CV: 0.11 – 0.17) being higher than that in the CO emission rate (CV:
439 0.07 – 0.14) according to REAS in China, and domestic heating is the main factor affecting the
440 seasonality. In contrast, the seasonal pattern in the REAS BC/CO ratios of South Korea and
441 Japan, higher in summer than in spring or winter, can be explained by the term of the CO
442 emission rate (CV: 0.05 for South Korea and 0.12 for Japan) compared to that of BC (CV: 0.005
443 for South Korea and 0.03 for Japan), which showed a relatively constant rate throughout the
444 year.

445 The average absolute MFB of $\Delta\text{BC}/\Delta\text{CO}$ between the recalculated REAS and the measured
446 values in all regions was 0.29, and that in spring was the lowest as 0.19, followed by winter
447 (0.33), fall (0.34) and summer (0.61). However, the MFB in summer decreased to 0.30, which

448 was close to that in fall and winter, when the low $\Delta BC/\Delta CO$ ratio in North China and Northeast
449 China was excluded due to the small number of data (≤ 50). The MFB in South Korea was too
450 high, ranging from 0.64 to 0.93, due to underestimation of the CO emission rate, as discussed
451 in section 3.3. It should be noted that the measured $\Delta BC/\Delta CO$ ratios in spring were the highest
452 among the seasons for all dominant emission regions except for North Korea; in particular,
453 those in East China, South Korea, and Japan showed significant differences in the $\Delta BC/\Delta CO$
454 ratios between spring and winter ($p \leq 0.05$). These higher $\Delta BC/\Delta CO$ ratios in spring than in
455 winter were also observed at Hedo, Okinawa (Verma et al., 2011). This difference might be
456 caused by the seasonality of BC emissions from the domestic sector between spring and winter,
457 which was overwhelmed by the seasonality of CO emissions. The annual consumption of coal
458 (high BC/CO ratios) for households was slightly decreased from 100.4 to 93.5 million tons,
459 whereas that of natural gas (non-emitted BC) showed a significant increase from 7.9 to 36
460 billion m^3 as a factor of 3.6 times from 2005 to 2015 (National Bureau of Statistics of China,
461 2017). This fuel transition for the domestic sector could have caused a decreased $\Delta BC/\Delta CO$
462 ratio in winter due to the constant BC emission rate along with increasing CO emission rate.

463 Although the $\Delta BC/\Delta CO$ in Japan showed good agreement with the regional REAS BC/CO
464 ratio, the mean absolute MFB was 0.30, which was not low, as we expected. In the REAS
465 emission inventory, the CO emission rates in South Korea and Japan mainly varied due to the
466 domestic sector and road transportation, respectively, and those rates were maximum in winter
467 and minimum in summer. The reason why the observed $\Delta BC/\Delta CO$ ratios in both South Korea
468 and Japan showed the highest values in spring and not summer is that the ratio of ΔBC in spring
469 to that in summer was higher than the corresponding ratio of ΔCO , implying that seasonal
470 variations in the CO emission rate could not represent the seasonal characteristics.

471 Similar to the regional variation, the seasonal variation of other inventories also showed
472 large differences not only in the variation pattern but also in magnitude (Figure S10). As
473 discussed for the regional variations of the emission inventory (section 3.3), the MIX inventory
474 showed similar seasonal variations to those of the REAS emission inventory, indicating high
475 BC/CO ratios in winter for China (due to residential heating) and high values in summer for
476 Japan (due to traffic). On the other hand, the seasonal variation of EDGAR reached the
477 maximum in summer for China and in winter for South Korea and Japan, which is an opposite
478 seasonal pattern to that of the REAS and MIX emission inventories. The reason why the

479 summer ratio was high in China is that the emission rates from industry increased in summer.
480 This tendency was prominent in North China due to the much higher BC/CO ratio (this was
481 especially relevant for oil refineries and the transformation industry). High BC/CO ratios in
482 winter in Korea and Japan were due to the reduced effect from road transportation, which has
483 a low BC/CO ratio.

485 **3.5 Estimated potential regions of over- and underestimation for $\Delta BC/\Delta CO$**

486 An investigation of the potential locations for over- and underestimated $\Delta BC/\Delta CO$ ratios
487 was performed using a potential source contribution function (PSCF). Typically, the PSCF has
488 been widely applied to identify source regions of aerosols on regional scales, as well as to
489 identify long-range transported pollution to a receptor site (Guo et al., 2015; Kim et al., 2016).
490 Unlike the grid size of the REAS emission inventory, the trajectory endpoints are assigned to
491 cells of $0.5^\circ \times 0.5^\circ$ geographic coordinates with a latitude (i) and longitude (j), and the number
492 of trajectory segment endpoints within the grid cell is counted. The PSCF at the ij th grid cell
493 can be calculated by the following:

$$494 \quad PSCF_{i,j} = \frac{\sum m_{i,j}}{\sum n_{i,j}}$$

495 where $n_{i,j}$ is the total number of trajectory endpoints over the ij th grid cell and $m_{i,j}$ is the
496 number of these endpoints that correspond to values higher or lower than certain criteria over
497 a certain grid cell. We applied MFB values higher than 0.5 and lower than -0.5 for over- and
498 underestimated criteria, respectively. If the total number of trajectory segment endpoints in a
499 particular cell ($\sum n_{i,j}$) is small, the PSCF value may be biased toward overestimation,
500 especially when the value of $\sum m_{i,j}$ is higher at the receptor site. To reduce the effect of
501 abnormal and large $PSCF_{ij}$ values with low $\sum n_{i,j}$, a weight function (Guo et al., 2015) was
502 applied with the power law of the total number of trajectories ($N_{APT=0}$ for each site in Table 2).

503 For overestimated cases ($MFB \geq 0.5$; Figure 5), South Korea was clearly identified as a
504 region with a higher PSCF value, regardless of the measurement site. In particular, the western
505 region of South Korea, including the SMA and the southwestern region, showed the highest
506 PSCF values. High PSCF values in Baengnyeong were observed in the SMA region (17.2 ng

507 $\text{m}^{-3} \text{ppb}^{-1}$ from REAS) with 0.60, whereas those in Gosan were located in the southwestern
508 region of Korea ($30.7 \text{ ng m}^{-3} \text{ppb}^{-1}$ from REAS) with 0.65, suggesting that the southwestern
509 region of Korea is more overestimated than the SMA region. Although the measured $\Delta\text{BC}/\Delta\text{CO}$
510 ratios were similar at Fukuoka and Noto, the overestimated region for Fukuoka was more
511 emphasized in SMA with a higher PSCF value (0.61) than that for Noto, which indicated that
512 the southeastern region ($27.0 \text{ ng m}^{-3} \text{ppb}^{-1}$ from REAS) had a relatively low PSCF (0.42). In
513 China, Liaoning ($10.8 \text{ ng m}^{-3} \text{ppb}^{-1}$ from REAS) in Northeast China revealed the highest PSCF
514 (0.43), followed by Tianjin ($7.0 \text{ ng m}^{-3} \text{ppb}^{-1}$ from REAS) in the North China at Baengnyeong,
515 along with similar results in Gosan. Fukuoka and Noto did not directly point out the
516 overestimation regions in China. Nonetheless, Noto may indicate that Heilongjiang (14.0 ng
517 $\text{m}^{-3} \text{ppb}^{-1}$) is related to a large overestimation of the ratio, as deduced from the pathway of
518 air mass toward Northeast China. For Japan, the Kyushu and central region (Kansai, Kanto, and
519 Chubu) showed moderate PSCF values (~ 0.3), implying relatively good consistency between
520 the REAS and the measured ratios.

521 On the other hand, a PSCF value higher than 0.2 for an underestimated case ($\text{MFB} \leq -0.5$,
522 Figure 6) was observed only at the Baengnyeong site for North Korea. The most
523 underestimated regions were identified as the western regions of North Korea, such as
524 Pyongyang ($4.72 \text{ ng m}^{-3} \text{ppb}^{-1}$ from REAS) and nearby. These regions showed the highest CO
525 emission rates (Figure 1), especially from the industrial sector, suggesting that the accuracies
526 of the CO emission rates from not only road transportation but also the industrial sector should
527 be improved. The results of PSCF analysis provided useful information on the potentially over-
528 and underestimated BC/CO ratio regions where the BC and CO emission rates should be
529 preferentially updated.

530

531 **4 Conclusions**

532 To verify the REAS bottom-up emission inventory, the $\Delta\text{BC}/\Delta\text{CO}$ ratios were diagnosed
533 from long-term, best-effort observations at four sites in East Asia, including two sites in Korea
534 (Baengnyeong and Gosan) and two sites in Japan (Fukuoka and Noto). Based on the backward
535 trajectories covering the past 72 hours, dominant emission regions were assigned to six study
536 domains divided by country and/or administrative district, including three Chinese regions

537 (East, North, and Northeast), two Korean peninsula regions (South and North Korea), and
538 Japan. To choose cases without wet deposition effects, the $\Delta BC/\Delta CO$ ratio was considered only
539 when the accumulated precipitation along a backward trajectory (APT) for three days was equal
540 to zero.

541 The regional $\Delta BC/\Delta CO$ ratios were overestimated in the REAS emission inventory from
542 East, North and Northeast China. The REAS BC/CO ratio of South Korea was 3.0 times higher
543 than the measured $\Delta BC/\Delta CO$ ratio, whereas Japan showed good consistency between the two
544 ratios. The plausible reason was that the CO emissions rates from gasoline vehicles and
545 motorcycles in South Korea were highly underestimated when considering hypothetical CO
546 emission factors compared to those in Japan. However, North Korea revealed a highly
547 underestimated region by a factor of 2.0 due to unrealistically overestimated CO emissions
548 from vehicles, although it is hard to directly compare these emissions with those in other
549 countries due to the possibility of differences in fuel usage and combustion technology. The
550 seasonal variation in the $\Delta BC/\Delta CO$ ratio revealed different tendencies. The BC/CO ratios from
551 REAS (and MIX) peaked in winter (China and North Korea) and in summer (South Korea and
552 Japan), which is an opposite seasonal pattern to that of EDGAR values. In contrast, the
553 measured ratio was the highest in spring, implying that the REAS and other emission
554 inventoryinventories did not reflect the major seasonality driver. From the PSCF analysis, the
555 potentially over- and underestimated regions were emphasized in the SMA and southwestern
556 regions of South Korea and Pyongyang of North Korea, respectively. In addition to the
557 highlighted regions in the Korean peninsula, moderate PSCF values for overestimation were
558 also observed at Tianjin (East), Liaoning and Heilongjiang (Northeast) in China and at Kyushu
559 and the central region in Japan.

560 This study provided the overall mean BC/CO ratio with uncertainty for each dominant
561 emission region by taking into consideration the full range of the $\Delta BC/\Delta CO$ ratio based on
562 spatial (four sites) and temporal variations (four seasons) (Table 3). The BC emissions over
563 East Asia can be estimated by multiplying the observed $\Delta BC/\Delta CO$ ratio by reliable estimates
564 of the CO emission rate. The discrepancy in the BC/CO ratio is largely contributed by
565 inaccurate CO emission rates in emission inventories, in addition to BC emission factors.
566 Therefore, to enhance the accuracy of the BC emission rate over East Asia, a comprehensive
567 and in-depth investigation of CO emissions should be performed to accurately assess the CO

568 emission rate by considering not only the annual total but also the monthly basis, particularly
569 in the Korean peninsula.

570

571 **Author contributions**

572 YC and YK designed the study and prepared the manuscript with contributions from all co-
573 authors. SMP, HK and DHJ were responsible for measurements at Baengnyeong. AM and YS
574 conducted measurements at Noto and IU provided the data at Fukuoka. SWK and ML
575 contributed to ground observations and quality control at Gosan. XP contributed the data
576 analysis. All co-authors provided professional comments to improve the manuscript.

577

578 **Acknowledgments**

579 This research was supported by the Environment Research and Technology Development
580 Fund (2-1803) of the Ministry of the Environment, Japan. The authors thank NOAA ARL for
581 providing the HYSPLIT backward trajectories.

582

583 **References**

- 584 [Bey, I., Jacob, D., Logan, J., and Yantosca, R.: Asian chemical outflow to the Pacific in](#)
585 [spring: Origins, pathways, and budgets, *J. Geophys. Res.-Atmos.*, 106, 23097–23113,](#)
586 [doi:10.1029/2001JD000806, 2001](#)
- 587 Bond, T. C., Anderson, T. L., and Campbell, D.: Calibration and Intercomparison of Filter-
588 Based Measurements of Visible Light Absorption by Aerosols, *Aerosol Sci. Technol.*, 30,
589 582-600, 10.1080/0278682993044435, 1999.
- 590 Bond, T. C., Doherty, S. J., Fahey, D., Forster, P., Berntsen, T., DeAngelo, B., Flanner, M.,
591 Ghan, S., Kärcher, B., and Koch, D.: Bounding the role of black carbon in the climate
592 system: A scientific assessment, *J. Geophys. Res. Atmos.*, 118, 5380-5552, 2013.
- 593 Cho, C., Kim, S.-W., Lee, M., Lim, S., Fang, W., Gustafsson, Ö., Andersson, A., Park, R. J.,
594 and Sheridan, P. J.: Observation-based estimates of the mass absorption cross-section of
595 black and brown carbon and their contribution to aerosol light absorption in East Asia,
596 *Atmos. Environ.*, 212, 65-74, <https://doi.org/10.1016/j.atmosenv.2019.05.024>, 2019.
- 597 Crippa, M., Guizzardi, D., Muntean, M., Schaaf, E., Dentener, F., van Aardenne, J. A.,
598 Monni, S., Doering, U., Olivier, J. G. J., Pagliari, V., and Janssens-Maenhout, G.: Gridded
599 emissions of air pollutants for the period 1970–2012 within EDGAR v4.3.2, *Earth Syst.*
600 *Sci. Data*, 10, 1987-2013, 10.5194/essd-10-1987-2018, 2018.

- 601 Draxler, R., Stunder, B., Rolph, G., Stein, A., Taylor, A.: HYSPLIT4 user's guide, version 4,
602 http://www.arl.noaa.gov/documents/reports/hysplit_user_guide.pdf, last access: 27 Jun
603 2019, 2018.
- 604 Geng, F., Hua, J., Mu, Z., Peng, L., Xu, X., Chen, R., and Kan, H.: Differentiating the
605 associations of black carbon and fine particle with daily mortality in a Chinese city,
606 *Environmental Research*, 120, 27-32, <https://doi.org/10.1016/j.envres.2012.08.007>, 2013.
- 607 Guo, Q., Hu, M., Guo, S., Wu, Z., Hu, W., Peng, J., Hu, W., Wu, Y., Yuan, B., Zhang, Q., and
608 Song, Y.: The identification of source regions of black carbon at a receptor site off the
609 eastern coast of China, *Atmos. Environ.*, 100, 78-84,
610 <http://dx.doi.org/10.1016/j.atmosenv.2014.10.053>, 2015.
- 611 Guo, Q., Hu, M., Guo, S., Wu, Z., Peng, J., and Wu, Y.: The variability in the relationship
612 between black carbon and carbon monoxide over the eastern coast of China: BC aging
613 during transport, *Atmos. Chem. Phys.*, 17, 10395-10403, [10.5194/acp-17-10395-2017](https://doi.org/10.5194/acp-17-10395-2017),
614 2017.
- 615 Han, S., Kondo, Y., Oshima, N., Takegawa, N., Miyazaki, Y., Hu, M., Lin, P., Deng, Z., Zhao,
616 Y., Sugimoto, N., and Wu, Y.: Temporal variations of elemental carbon in Beijing, *J.*
617 *Geophys. Res. Atmos.*, 114, [doi:10.1029/2009JD012027](https://doi.org/10.1029/2009JD012027), 2009.
- 618 [Han, K. M., Lee, S., Chang, L. S., and Song, C. H.: A comparison study between CMAQ-](https://doi.org/10.5194/acp-15-1913-2015)
619 [simulated and OMI-retrieved NO₂ columns over East Asia for evaluation of NO_x](https://doi.org/10.5194/acp-15-1913-2015)
620 [emission fluxes of INTEX-B, CAPSS, and REAS inventories, *Atmos. Chem. Phys.*, 15,](https://doi.org/10.5194/acp-15-1913-2015)
621 [1913-1938, <https://doi.org/10.5194/acp-15-1913-2015>, 2015.](https://doi.org/10.5194/acp-15-1913-2015)
- 622 Huebert, B. J., Bates, T., Russell, P. B., Shi, G., Kim, Y. J., Kawamura, K., Carmichael, G.,
623 and Nakajima, T.: An overview of ACE-Asia: Strategies for quantifying the relationships
624 between Asian aerosols and their climatic impacts, *J. Geophys. Res. Atmos.*, 108,
625 [doi:10.1029/2003JD003550](https://doi.org/10.1029/2003JD003550), 2003.
- 626 Itahashi, S., Uno, I., Osada, K., Kamiguchi, Y., Yamamoto, S., Tamura, K., Wang, Z.,
627 Kurosaki, Y., and Kanaya, Y.: Nitrate transboundary heavy pollution over East Asia in
628 winter, *Atmos. Chem. Phys.*, 17, 3823-3843, [10.5194/acp-17-3823-2017](https://doi.org/10.5194/acp-17-3823-2017), 2017.
- 629 Jacobson, M. Z.: Strong radiative heating due to the mixing state of black carbon in
630 atmospheric aerosols, *Nature*, 409, 695, [10.1038/35055518](https://doi.org/10.1038/35055518).
- 631 Janssen, N., A. H., Hoek, G., Simic-Lawson, M., Fischer, P., van Bree, L., ten Brink, H.,
632 Keuken, M., Atkinson Richard, W., Anderson, H. R., Brunekreef, B., and Cassee
633 Flemming, R.: Black Carbon as an Additional Indicator of the Adverse Health Effects of
634 Airborne Particles Compared with PM₁₀ and PM_{2.5}, *Environ. Health Perspect.*, 119,
635 1691-1699, [10.1289/ehp.1003369](https://doi.org/10.1289/ehp.1003369), 2011.
- 636 Janssen, N. A., Gerlofs-Nijland, M. E., Lanki, T., Salonen, R. O., Cassee, F., Hoek, G.,
637 Fischer, P., Brunekreef, B., and Krzyzanowski, M.: Health effects of black carbon, WHO
638 Regional Office for Europe Copenhagen, 2012.
- 639 Kanaya, Y., Komazaki, Y., Pochanart, P., Liu, Y., Akimoto, H., Gao, J., Wang, T., and Wang,
640 Z.: Mass concentrations of black carbon measured by four instruments in the middle of
641 Central East China in June 2006, *Atmos. Chem. Phys.*, 8, 7637-7649, [10.5194/acp-8-](https://doi.org/10.5194/acp-8-7637-2008)
642 [7637-2008](https://doi.org/10.5194/acp-8-7637-2008), 2008.

- 643 Kanaya, Y., Taketani, F., Komazaki, Y., Liu, X., Kondo, Y., Sahu, L. K., Irie, H., and
644 Takashima, H.: Comparison of Black Carbon Mass Concentrations Observed by Multi-
645 Angle Absorption Photometer (MAAP) and Continuous Soot-Monitoring System
646 (COSMOS) on Fukue Island and in Tokyo, Japan, *Aerosol Sci. Technol.*, 47, 1-10,
647 10.1080/02786826.2012.716551, 2013.
- 648 Kanaya, Y., Pan, X., Miyakawa, T., Komazaki, Y., Taketani, F., Uno, I., and Kondo, Y.: Long-
649 term observations of black carbon mass concentrations at Fukue Island, western Japan,
650 during 2009–2015: constraining wet removal rates and emission strengths from East Asia,
651 *Atmos. Chem. Phys.*, 16, 10689-10705, 10.5194/acp-16-10689-2016, 2016.
- 652 Kim, B. M., Seo, J., Kim, J. Y., Lee, J. Y., and Kim, Y.: Transported vs. local contributions
653 from secondary and biomass burning sources to PM_{2.5}, *Atmos. Environ.*, 144, 24-36,
654 <https://doi.org/10.1016/j.atmosenv.2016.08.072>, 2016.
- 655 Kim, I. S., and Kim, Y. P.: Characteristics of Energy Usage and Emissions of Air Pollutants in
656 North Korea, *J. Korean Soc. Atmos. Environ.*, 35, 125-137, 2019.
- 657 Kondo, Y., Komazaki, Y., Miyazaki, Y., Moteki, N., Takegawa, N., Kodama, D., Deguchi, S.,
658 Nogami, M., Fukuda, M., Miyakawa, T., Morino, Y., Koike, M., Sakurai, H., and Ehara,
659 K.: Temporal variations of elemental carbon in Tokyo, *J. Geophys. Res. Atmos.*, 111,
660 doi:10.1029/2005JD006257, 2006.
- 661 [Kondo, Y., Sahu, L., Moteki, N., Khan, F., Takegawa, N., Liu, X., Koike, M., and Miyakawa,](#)
662 [T.: Consistency and Traceability of Black Carbon Measurements Made by Laser-Induced](#)
663 [Incandescence, Thermal-Optical Transmittance, and Filter-Based Photo-Absorption](#)
664 [Techniques, *Aerosol Sci. Tech.*, 45, 295-312, 10.1080/02786826.2010.533215, 2011.](#)
- 665 Kondo, Y.: Effects of black carbon on climate: Advances in measurement and modeling,
666 *Monogr. Environ. Earth Planets*, 3, 1-85, 2015.
- 667 Kurokawa, J., Ohara, T., Morikawa, T., Hanayama, S., Janssens-Maenhout, G., Fukui, T.,
668 Kawashima, K., and Akimoto, H.: Emissions of air pollutants and greenhouse gases over
669 Asian regions during 2000–2008: Regional Emission inventory in ASia (REAS) version
670 2, *Atmos. Chem. Phys.*, 13, 11019-11058, 10.5194/acp-13-11019-2013, 2013.
- 671 Li, M., Zhang, Q., Kurokawa, J. I., Woo, J. H., He, K., Lu, Z., Ohara, T., Song, Y., Streets, D.
672 G., Carmichael, G. R., Cheng, Y., Hong, C., Huo, H., Jiang, X., Kang, S., Liu, F., Su, H.,
673 and Zheng, B.: MIX: a mosaic Asian anthropogenic emission inventory under the
674 international collaboration framework of the MICS-Asia and HTAP, *Atmos. Chem. Phys.*,
675 17, 935-963, 10.5194/acp-17-935-2017, 2017.
- 676 Lim, S., Lee, M., Lee, G., Kim, S., Yoon, S., and Kang, K.: Ionic and carbonaceous
677 compositions of PM₁₀, PM_{2.5} and PM_{1.0} at Gosan ABC Superstation and their ratios as
678 source signature, *Atmos. Chem. Phys.*, 12, 2007-2024, 10.5194/acp-12-2007-2012, 2012.
- 679 Loomis, D., Grosse, Y., Lauby-Secretan, B., Ghissassi, F. E., Bouvard, V., Benbrahim-Tallaa,
680 L., Guha, N., Baan, R., Mattock, H., and Straif, K.: The carcinogenicity of outdoor air
681 pollution, *Lancet Oncol.*, 14, 1262-1263, [https://doi.org/10.1016/S1470-2045\(13\)70487-](https://doi.org/10.1016/S1470-2045(13)70487-X)
682 [X](https://doi.org/10.1016/S1470-2045(13)70487-X), 2013.
- 683 [Matsui, H., Kondo, Y., Moteki, N., Takegawa, N., Sahu, L. K., Zhao, Y., Fuelberg, H. E.,](#)
684 [Sessions, W. R., Diskin, G., Blake, D. R., Wisthaler, A., and Koike, M.: Seasonal](#)

- 685 [variation of the transport of black carbon aerosol from the Asian continent to the Arctic](#)
686 [during the ARCTAS aircraft campaign, *Journal of Geophysical Research: Atmospheres*,](#)
687 [116, 10.1029/2010JD015067, 2011.](#)
- 688 Miyakawa, T., Oshima, N., Taketani, F., Komazaki, Y., Yoshino, A., Takami, A., Kondo, Y.,
689 and Kanaya, Y.: Alteration of the size distributions and mixing states of black carbon
690 through transport in the boundary layer in east Asia, *Atmos. Chem. Phys.*, 17, 5851-5864,
691 10.5194/acp-17-5851-2017, 2017.
- 692 [Miyakawa, T., Kanaya, Y., Komazaki, Y., Taketani, F., Pan, X., Irwin, M., and Symonds, J.:](#)
693 [Intercomparison between a single particle soot photometer and evolved gas analysis in an](#)
694 [industrial area in Japan: Implications for the consistency of soot aerosol mass](#)
695 [concentration measurements, *Atmos. Environ.*, 127, 14-21,](#)
696 <https://doi.org/10.1016/j.atmosenv.2015.12.018>, 2016.
- 697 Miyazaki, K., Sekiya, T., Fu, D., Bowman, K. W., Kulawik, S. S., Sudo, K., Walker, T.,
698 Kanaya, Y., Takigawa, M., Ogochi, K., Eskes, H., Boersma, K. F., Thompson, A. M.,
699 Gaubert, B., Barre, J., and Emmons, L. K.: Balance of Emission and Dynamical Controls
700 on Ozone During the Korea-United States Air Quality Campaign From Multiconstituent
701 Satellite Data Assimilation, *J. Geophys. Res. Atmos.*, 124, 387-413,
702 doi:10.1029/2018JD028912, 2019.
- 703 MLIT (Ministry of Land, Infrastructure, Transport and Tourism): Annual report of
704 Automobile transportation statistics in 2015, [https://www.e-stat.go.jp/stat-search/file-](https://www.e-stat.go.jp/stat-search/file-download?statInfId=000031752810&fileKind=2)
705 [download?statInfId=000031752810&fileKind=2](https://www.e-stat.go.jp/stat-search/file-download?statInfId=000031752810&fileKind=2), last access: 25 Jan 2019, 2016 (in
706 Japanese).
- 707 MLIT: Traffic statistics book, <http://www.mlit.go.jp/statistics/kotsusiryu.html>, last access: 27
708 June 2019 (in Japanese).
- 709 MOLIT (Ministry of Land, Infrastructure and Transport): Total Registered Moter Vehicles,
710 <http://stat.molit.go.kr/portal/cate/statFileView.do?hRsId=58&hFormId=5...>, last access: 8
711 Feb 2019 (in Korean).
- 712 Myhre, G., Shindell, D., Bréon, F.-M., Collins, W., Fuglestedt, J., Huang, J., Koch, D.,
713 Lamarque, J.-F., Lee, D., and Mendoza, B., Nakajima, T., Robock, A., Stephens, G.,
714 Takemura, T., and Zhang, H.: Anthropogenic and Natural Radiative Forcing. In: *Climate*
715 *Change 2013: The Physical Science Basis. Contribution of Working Group I to the Fifth*
716 *Assessment Report of the Intergovernmental Panel on Climate Change*, Cambridge
717 University Press, Cambridge, United Kingdom and New York, NY, USA, 2013.
- 718 Nakajima, T., Yoon, S.-C., Ramanathan, V., Shi, G.-Y., Takemura, T., Higurashi, A.,
719 Takamura, T., Aoki, K., Sohn, B.-J., Kim, S.-W., Tsuruta, H., Sugimoto, N., Shimizu, A.,
720 Tanimoto, H., Sawa, Y., Lin, N.-H., Lee, C.-T., Goto, D., and Schutgens, N.: Overview of
721 the Atmospheric Brown Cloud East Asian Regional Experiment 2005 and a study of the
722 aerosol direct radiative forcing in east Asia, *J. Geophys. Res. Atmos.*, 112,
723 doi:10.1029/2007JD009009, 2007.
- 724 National Bureau of Statistics of China: *China Statistical Yearbook 2017*, China Statistics
725 Press, Beijing, ISBN-13: 978-7503782534, 2017.
- 726 NIOSH: Method 5040 issue 1: elemental carbon (diesel exhaust), 4th ed., Cincinnati, OH,

- 727 1996.
- 728 Ogren, J. A., Wendell, J., Andrews, E., and Sheridan, P. J.: Continuous light absorption
729 photometer for long-term studies, *Atmos. Meas. Tech.*, 10, 4805-4818,
730 <https://doi.org/10.5194/amt-10-4805-2017>, 2017.
- 731 Ohara, T., Akimoto, H., Kurokawa, J., Horii, N., Yamaji, K., Yan, X., and Hayasaka, T.: An
732 Asian emission inventory of anthropogenic emission sources for the period
733 1980–2020, *Atmos. Chem. Phys.*, 7, 4419-4444, 10.5194/acp-7-4419-2007, 2007.
- 734 [Ohata, S., Kondo, Y., Moteki, N., Mori, T., Yoshida, A., Sinha, P. R., and Koike, M.:
735 Accuracy of black carbon measurements by a filter-based absorption photometer with a
736 heated inlet, *Aerosol Sci. Tech.*, 53, 1079-1091, 10.1080/02786826.2019.1627283, 2019.](#)
- 737 Oshima, N., Kondo, Y., Moteki, N., Takegawa, N., Koike, M., Kita, K., Matsui, H., Kajino,
738 M., Nakamura, H., Jung, J. S., and Kim, Y. J.: Wet removal of black carbon in Asian
739 outflow: Aerosol Radiative Forcing in East Asia (A-FORCE) aircraft campaign, *J.
740 Geophys. Res. Atmos.*, 117, 10.1029/2011JD016552, 2012.
- 741 Pan, X. L., Kanaya, Y., Wang, Z. F., Liu, Y., Pochanart, P., Akimoto, H., Sun, Y. L., Dong, H.
742 B., Li, J., Irie, H., and Takigawa, M.: Correlation of black carbon aerosol and carbon
743 monoxide in the high-altitude environment of Mt. Huang in Eastern China, *Atmos. Chem.
744 Phys.*, 11, 9735-9747, 10.5194/acp-11-9735-2011, 2011.
- 745 Pan, X. L., Kanaya, Y., Wang, Z. F., Komazaki, Y., Taketani, F., Akimoto, H., and Pochanart,
746 P.: Variations of carbonaceous aerosols from open crop residue burning with transport and
747 its implication to estimate their lifetimes, *Atmos. Environ.*, 74, 301-310,
748 <https://doi.org/10.1016/j.atmosenv.2013.03.048>, 2013.
- 749 [Park, R. J., Jacob, D. J., Palmer, P. I., Clarke, A. D., Weber, R. J., Zondlo, M. A., Eisele, F. L.,
750 Bandy, A. R., Thornton, D. C., Sachse, G.W., and Bond, T. C.: Export efficiency of black
751 carbon aerosol in continental outflow: Global implications, *J. Geophys. Res.-Atmos.*, 110,
752 1–7, <https://doi.org/10.1029/2004JD005432>, 2005.](#)
- 753 Park, S.-S., Jung, S.-A., Gong, B.-J., Cho, S.-Y., and Lee, S.-J.: Characteristics of PM2.5
754 Haze Episodes Revealed by Highly Time-Resolved Measurements at an Air Pollution
755 Monitoring Supersite in Korea, *Aerosol Air Qual. Res.*, 13, 957-976,
756 10.4209/aaqr.2012.07.0184, 2013.
- 757 Petzold, A., Schloesser, H., Sheridan, P. J., Arnott, W. P., Ogren, J. A., and Virkkula, A.:
758 Evaluation of Multiangle Absorption Photometry for Measuring Aerosol Light
759 Absorption, *Aerosol Sci. Technol.*, 39, 40-51, 10.1080/027868290901945, 2005.
- 760 Ramana, M. V., Ramanathan, V., Feng, Y., Yoon, S. C., Kim, S. W., Carmichael, G. R., and
761 Schauer, J. J.: Warming influenced by the ratio of black carbon to sulphate and the black-
762 carbon source, *Nature Geoscience*, 3, 542–545, , 2010.
- 763 Ramanathan, V., and Carmichael, G.: Global and regional climate changes due to black
764 carbon, *Nature Geoscience*, 1, 221, 10.1038/ngeo156, 2008.
- 765 Sahu, L. K., Kondo, Y., Miyazaki, Y., Kuwata, M., Koike, M., Takegawa, N., Tanimoto, H.,
766 Matsueda, H., Yoon, S. C., and Kim, Y. J.: Anthropogenic aerosols observed in Asian
767 continental outflow at Jeju Island, Korea, in spring 2005, *J. Geophys. Res. Atmos.*, 114,

768 doi:10.1029/2008JD010306, 2009.

769 Saikawa, E., Kim, H., Zhong, M., Avramov, A., Zhao, Y., Janssens-Maenhout, G., Kurokawa,
770 J.-I., Klimont, Z., Wagner, F., Naik, V., Horowitz, L. W., and Zhang, Q.: Comparison of
771 emissions inventories of anthropogenic air pollutants and greenhouse gases in China,
772 Atmos. Chem. Phys., 17, 6393–6421, <https://doi.org/10.5194/acp-17-6393-2017>, 2017.

773 Samset, B. H.: How cleaner air changes the climate, *Science*, 360, 148-150,
774 10.1126/science.aat1723, 2018.

775 Smith, K. R., Jerrett, M., Anderson, H. R., Burnett, R. T., Stone, V., Derwent, R., Atkinson, R.
776 W., Cohen, A., Shonkoff, S. B., Krewski, D., Pope, C. A., Thun, M. J., and Thurston, G.:
777 Public health benefits of strategies to reduce greenhouse-gas emissions: health
778 implications of short-lived greenhouse pollutants, *The Lancet*, 374, 2091-2103,
779 [https://doi.org/10.1016/S0140-6736\(09\)61716-5](https://doi.org/10.1016/S0140-6736(09)61716-5), 2009.

780 Su, L., Yuan, Z., Fung, J. C. H., and Lau, A. K. H.: A comparison of HYSPLIT backward
781 trajectories generated from two GDAS datasets, *Sci. Total Environ.*, 506-507, 527-537,
782 <https://doi.org/10.1016/j.scitotenv.2014.11.072>, 2015.

783 Statics of Korea: Major Statistics Indicators of North Korea, Statistics Korea, Korea, 287pp,
784 2017.

785 Taketani, F., Kanaya, Y., Nakayama, T., Ueda, S., Matsumi, Y., Sadanaga, Y., Iwamoto, Y.,
786 and Matsuki, A.: Property of Black Carbon Particles Measured by a Laser-Induced
787 Incandescence Technique in the spring at Noto Peninsula, Japan, *J. Aerosol Res.*, 31, 194-
788 202, 10.11203/jar.31.194, 2016 (Abstract in English).

789 Turpin, B. J., Saxena, P., and Andrews, E.: Measuring and simulating particulate organics in
790 the atmosphere: problems and prospects, *Atmos. Environ.*, 34, 2983-3013,
791 [https://doi.org/10.1016/S1352-2310\(99\)00501-4](https://doi.org/10.1016/S1352-2310(99)00501-4), 2000.

792 TS (Korea Transportation Safety Authority): A research on the real condition of driving
793 mileage in 2008,
794 <https://www.kotems.or.kr/app/kotems/forward?pageUrl=/kotems/ptl/bbs/KotemsPtlBbsSt>
795 [atsLs&topmenu1=06&topmenu2=03&topmenu3=03](https://www.kotems.or.kr/app/kotems/forward?pageUrl=/kotems/ptl/bbs/KotemsPtlBbsSt), last access: 25 Jun 2019, 2009 (In
796 Korean).

797 TS: A research on the real condition of actual driving mileage in 2015 (2012-2015),
798 <https://www.kotems.or.kr/app/kotems/forward?pageUrl=/kotems/ptl/bbs/KotemsPtlBbsSt>
799 [atsLs&topmenu1=06&topmenu2=03&topmenu3=03](https://www.kotems.or.kr/app/kotems/forward?pageUrl=/kotems/ptl/bbs/KotemsPtlBbsSt), last access: 25 Jun 2019, 2016 (In
800 Korean).

801 Ueda, S., Nakayama, T., Taketani, F., Adachi, K., Matsuki, A., Iwamoto, Y., Sadanaga, Y., and
802 Matsumi, Y.: Light absorption and morphological properties of soot-containing aerosols
803 observed at an East Asian outflow site, Noto Peninsula, Japan, *Atmos. Chem. Phys.*, 16,
804 2525-2541, 10.5194/acp-16-2525-2016, 2016.

805 Uno, I., Osada, K., Yumimoto, K., Wang, Z., Itahashi, S., Pan, X., Hara, Y., Kanaya, Y.,
806 Yamamoto, S., and Fairlie, T. D.: Seasonal variation of fine- and coarse-mode nitrates and
807 related aerosols over East Asia: synergetic observations and chemical transport model
808 analysis, *Atmos. Chem. Phys.*, 17, 14181-14197, 10.5194/acp-17-14181-2017, 2017.

- 809 Verma, R. L., Kondo, Y., Oshima, N., Matsui, H., Kita, K., Sahu, L. K., Kato, S., Kajii, Y.,
810 Takami, A., and Miyakawa, T.: Seasonal variations of the transport of black carbon and
811 carbon monoxide from the Asian continent to the western Pacific in the boundary layer, *J.*
812 *Geophys. Res. Atmos.*, 116, doi:10.1029/2011JD015830, 2011.
- 813 Wang, Y., Wang, X., Kondo, Y., Kajino, M., Munger, J. W., and Hao, J.: Black carbon and its
814 correlation with trace gases at a rural site in Beijing: Top-down constraints from ambient
815 measurements on bottom-up emissions, *J. Geophys. Res. Atmos.*, 116,
816 doi:10.1029/2011JD016575, 2011.
- 817 Woo, J.-H., Choi, K.-C., Kim, H. K., Baek, B. H., Jang, M., and Eum, J.-H.: Development of
818 an anthropogenic emissions processing system for Asia using SMOKE. *Atmos. Environ.*,
819 58, 5-13, 2012.
- 820 Woo, J.-H., Quan, S., Choi, K.-C., Kook, H., Jin, H., Song, C.-K., Han, J., and Lee, S.:
821 Development of the CREATE inventory in support of integrated modeling of climate and
822 air quality for East Asia, GEIA Conference, Boulder, USA, 2014.
- 823 Yeo, S.-Y., Lee, H.-K., Choi, S.-W., Seol, S.-H., Jin, H.-A., Yoo, C., Lim, J.-Y., and Kim, J.-
824 S.: Analysis of the National Air Pollutant Emission Inventory (CAPSS 2015) and the
825 Major Cause of Change in Republic of Korea, *Asian J. Atmos. Environ.*, 13, 212-231,
826 2019.
- 827 Yu, G. H., Park, S. S., Ghim, Y. S., Shin, H. J., Lim, C. S., Ban, S. J., Yu, J. A., Kang, H. J.,
828 Seo, Y. K., Kang, K. S., Jo, M. R., Jung, S. A., Lee, M. H., Hwang, T. K., Kang, B. C.,
829 and Kim, H. S.: Difference in Chemical Composition of PM_{2.5} and Investigation of its
830 Causing Factors between 2013 and 2015 in Air Pollution Intensive Monitoring Stations, *J.*
831 *Korean Soc. Atmos. Environ.*, 34, 16-37, 2018.
- 832 Zhou, X., Gao, J., Wang, T., Wu, W., and Wang, W.: Measurement of black carbon aerosols
833 near two Chinese megacities and the implications for improving emission inventories,
834 *Atmos. Environ.*, 43, 3918-3924, <https://doi.org/10.1016/j.atmosenv.2009.04.062>, 2009.
- 835 Zhu, C., Kanaya, Y., Yoshikawa-Inoue, H., Irino, T., Seki, O., and Tohjima, Y.: Sources of
836 atmospheric black carbon and related carbonaceous components at Rishiri Island, Japan:
837 The roles of Siberian wildfires and of crop residue burning in China, *Environ. Pollut.*,
838 247, 55-63, <https://doi.org/10.1016/j.envpol.2019.01.003>, 2019.

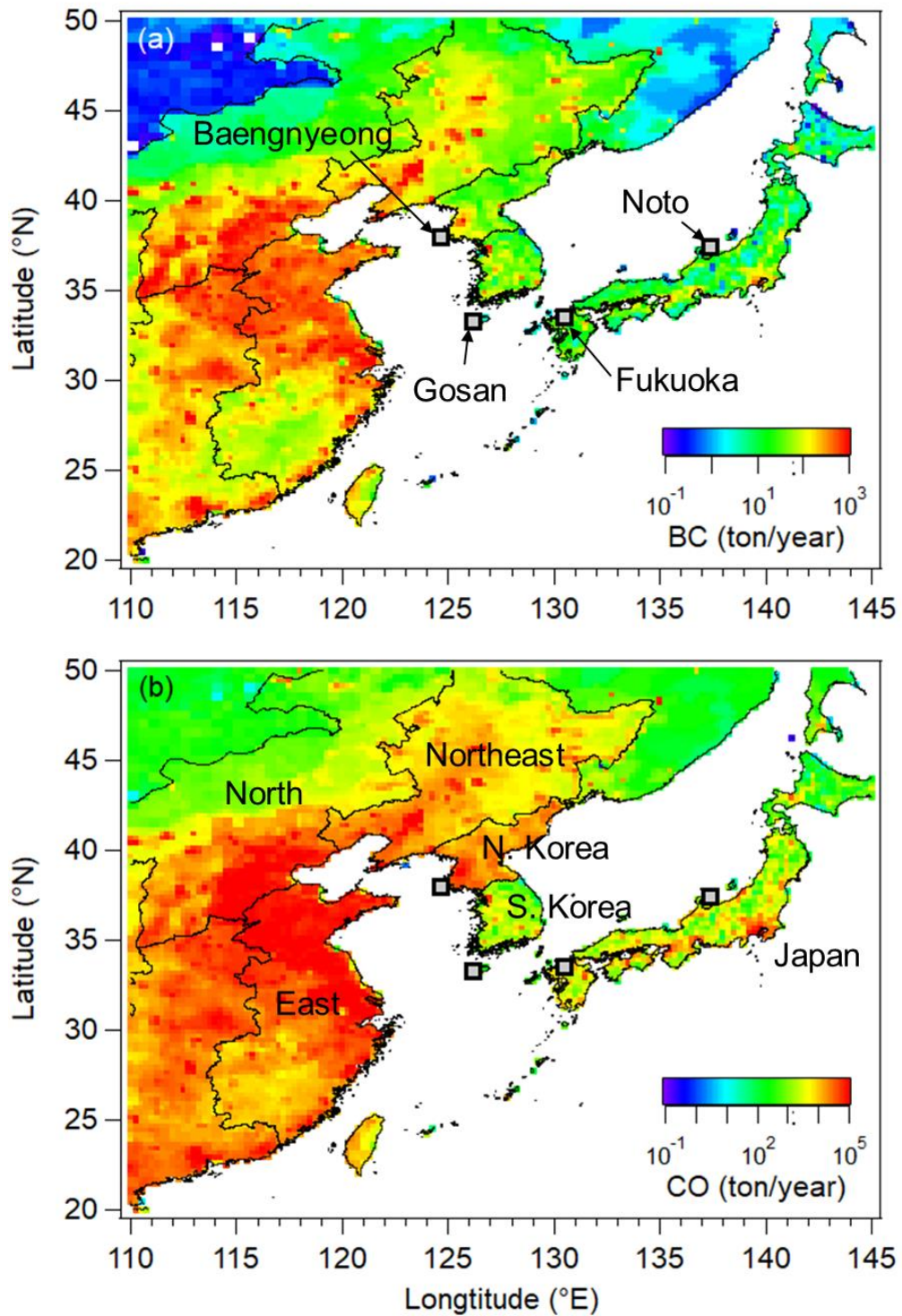


Figure 1. Yearly (a) BC and (b) CO emission rates (ton/year) over East Asia in 2008 from the REAS 2.1 bottom-up emission inventory (Kurokawa et al., 2013). The four measurement sites are shown in (a). (b) shows that the six study domains are divided by country and/or administrative district, including three Chinese regions (East, North, and Northeast), two Korean peninsula regions (South and North Korea), and Japan.

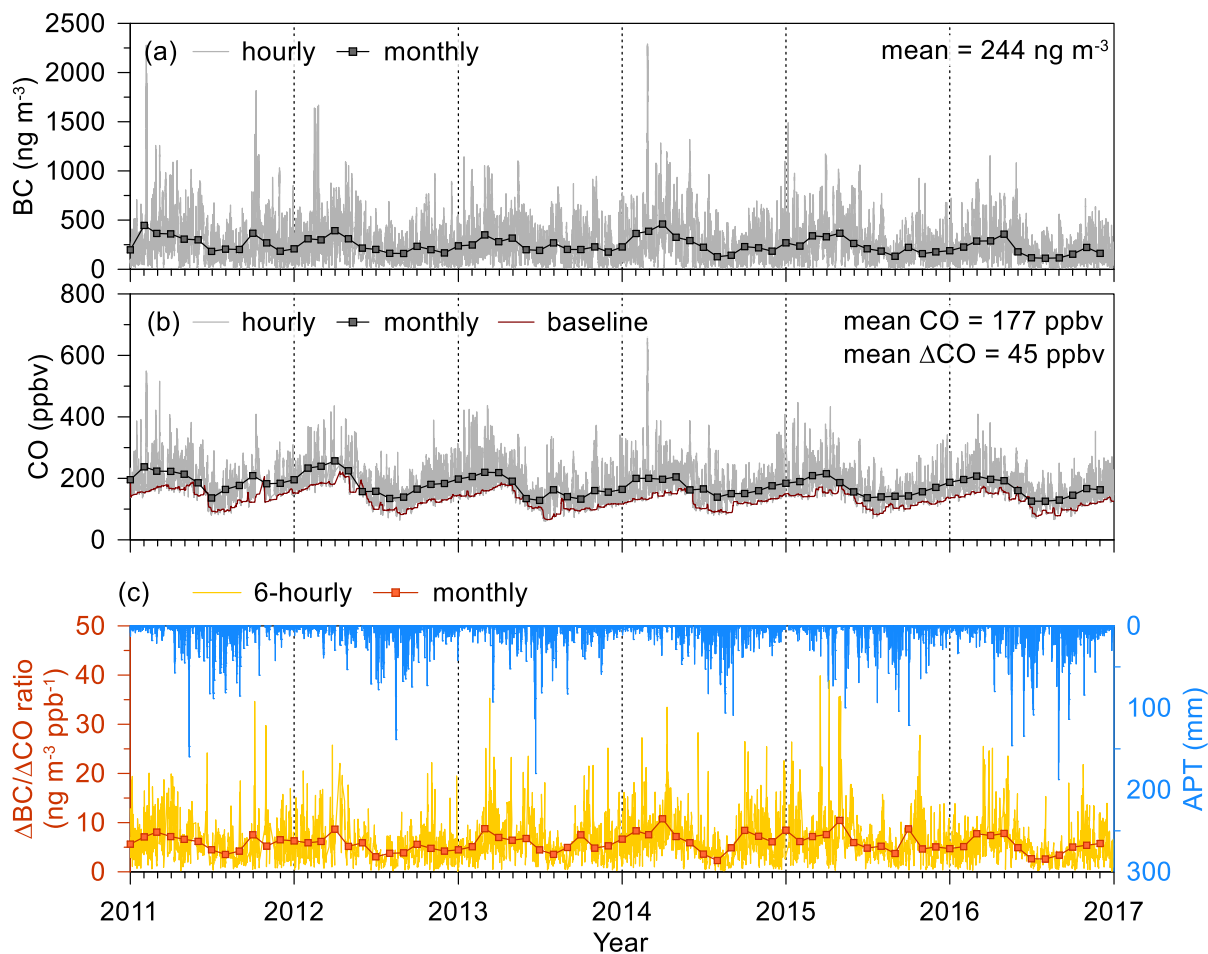


Figure 2. Time series of (a) BC concentration, (b) CO and ΔCO concentrations and (c) $\Delta\text{BC}/\Delta\text{CO}$ ratio and accumulated precipitation along with trajectory (APT), during the measurement periods (from 2011 to 2017) in Noto, Japan. The square symbols with solid lines in (a) and (b) indicate hourly and monthly concentrations.

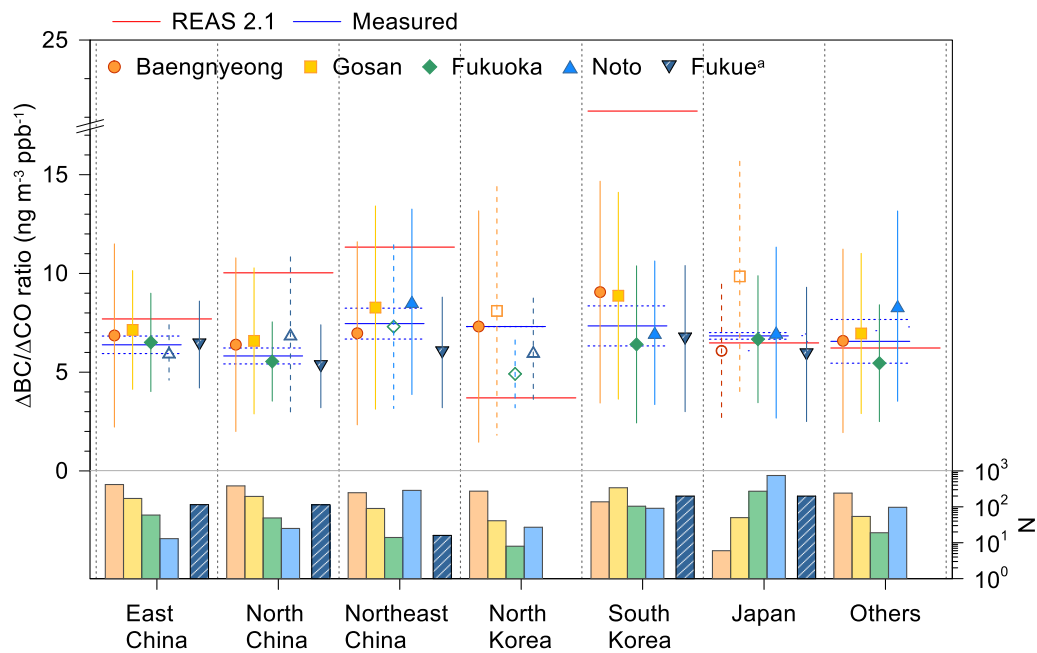


Figure 3. $\Delta BC/\Delta CO$ ratios at the four measurement sites and Fukue from Kanaya et al. (2016) according to the dominant emission region. The symbols with vertical lines are the means and standard deviations of the $\Delta BC/\Delta CO$ ratio. The bar graph on the bottom indicates the number of data in the dominant emission region. Open symbols with dashed vertical lines indicate data excluded because of a low number of data. The solid blue horizontal lines with dashed lines for each region indicate the means and standard deviations of the measured $\Delta BC/\Delta CO$, excluding the areas with limited data. The solid red horizontal lines depict the overall mean BC/CO ratios of dominant emission regions from the REAS version 2.1 emission inventory (Kurokawa et al., 2013).

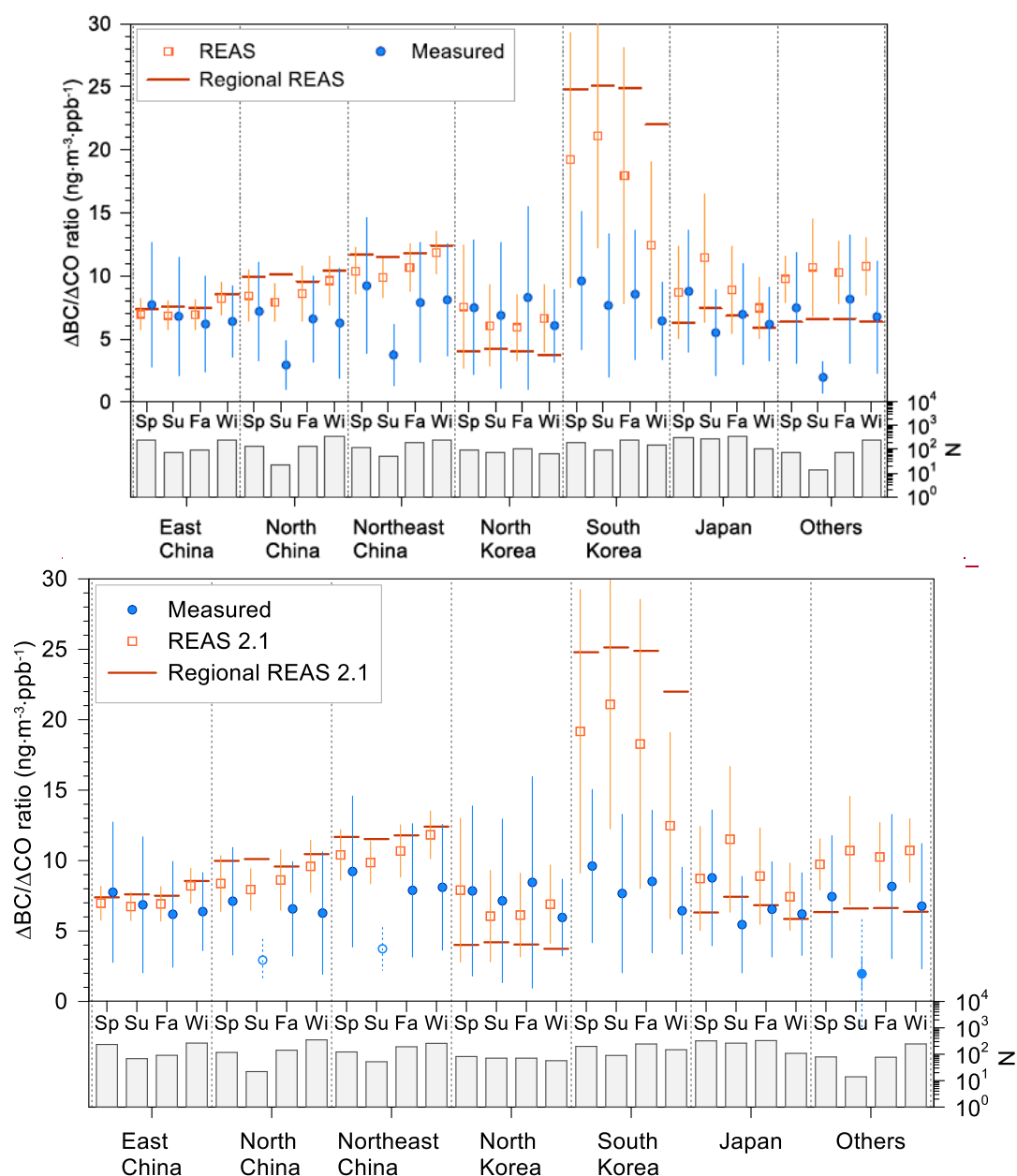


Figure 4. The seasonal $\Delta\text{BC}/\Delta\text{CO}$ ratios from four measurement sites (filled blue circles) and recalculated REAS BC/CO ratios according to the pathway of the trajectory (open orange squares), depending on the dominant emission region. The symbols with vertical lines are the means and standard deviations of the $\Delta\text{BC}/\Delta\text{CO}$ ratios. Open-circle symbols with dashed vertical lines indicate data excluded because of a low number of data (≤ 50). The horizontal lines for each region indicate the overall mean values of the $\Delta\text{BC}/\Delta\text{CO}$ ratios of dominant emission regions from the REAS version 2.1 emission inventory (Kurokawa et al., 2013). The bar graph on the bottom indicates the number of data in each season and the dominant emission region. The symbols with vertical lines are the means and standard deviations of the $\Delta\text{BC}/\Delta\text{CO}$ ratios. The abbreviation of ‘Sp’ to ‘Wi’ indicates spring to winter.

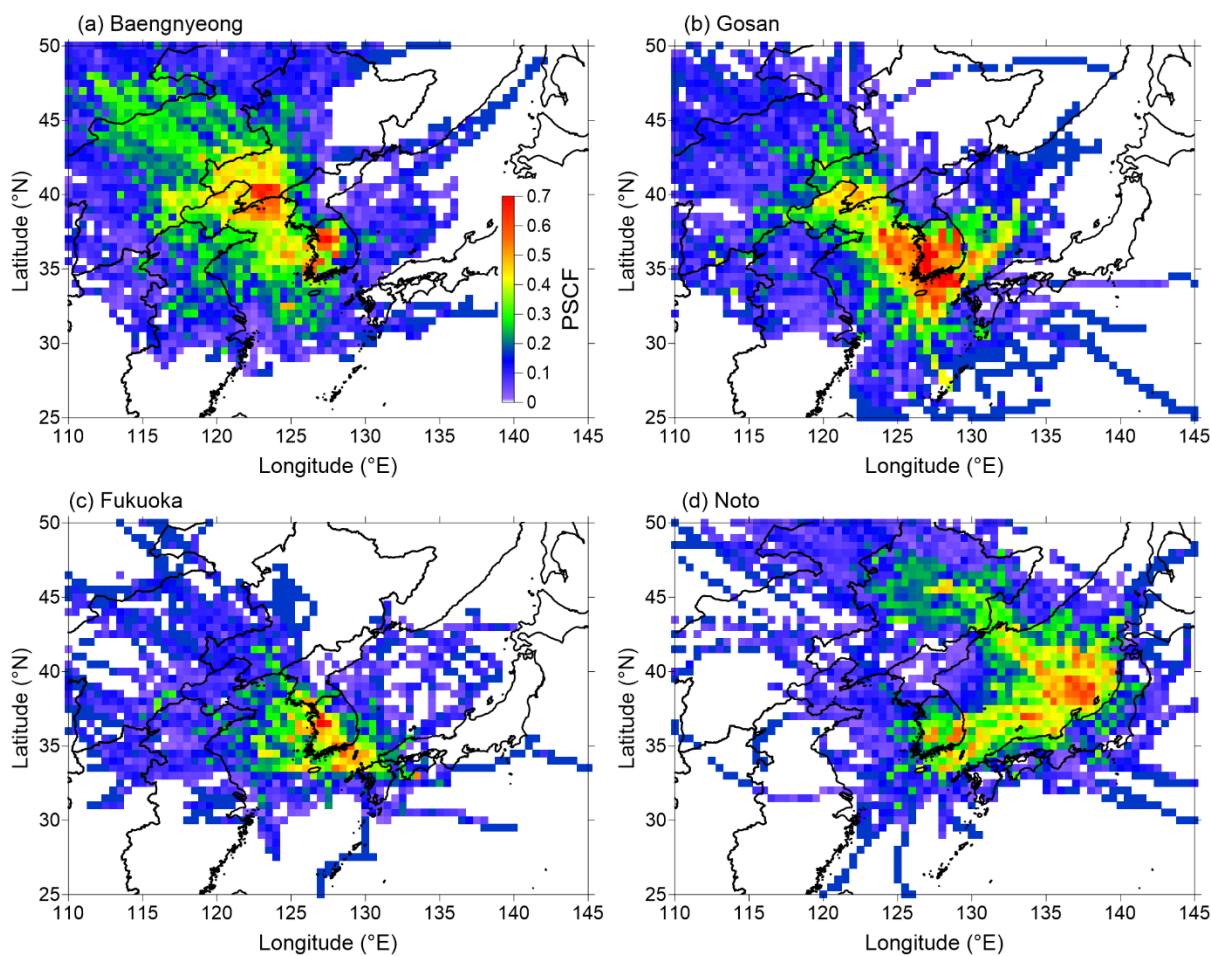


Figure 5. Spatial distribution of the PSCF results for the mean fractional bias (MFB) ≥ 0.5 for overestimation cases at the (a) Baengnyeong, (b) Gosan, (c) Fukuoka, and (d) Noto sites. MFB is calculated from $2 \times (R_i - M_i) / (R_i + M_i)$, where R_i and M_i denote the mean values of the recalculated REAS BC/CO ratio along with the backward trajectory and the measured BC/CO ratio, respectively.

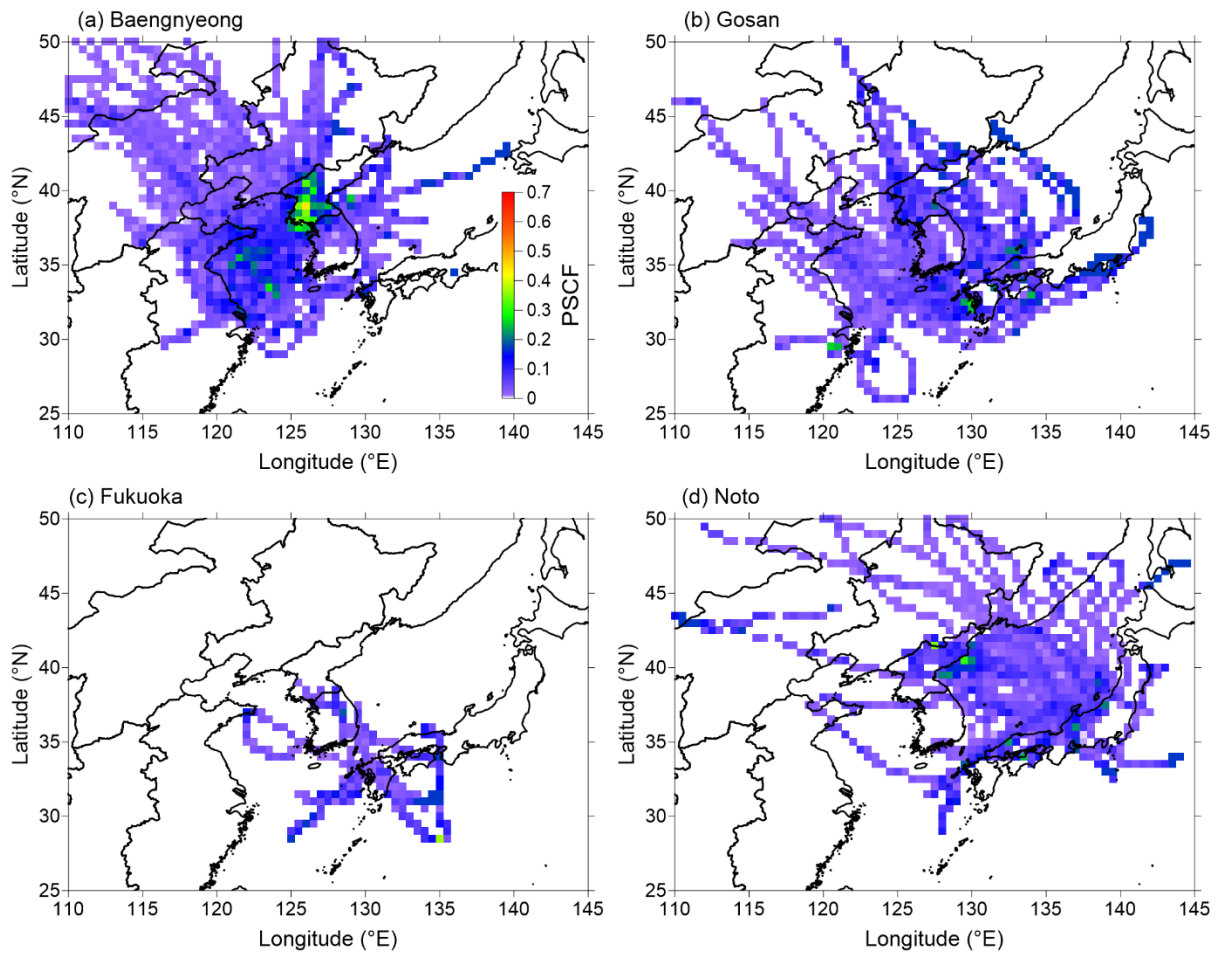


Figure 6. Same as Figure 5, except for the mean fractional bias (MFB) ≤ -0.5 for underestimation cases.

Table 1. Description of the measurement sites, periods, and instruments.

Sites		Longitude, Latitude	Measurement periods	Instruments
South Korea	Baengnyeong (background)	124.63 °E, 37.97 °N	2010.01.01 – 2016.12.31 (except for 2011 and 2012)	EC: sunset EC/OC (<u>PM_{2.5}</u>) CO: Teledyne API 300E
	Gosan (background)	126.17 °E, 33.28 °N	2012.05.01 – 2015.4.30	BC: CLAP ^a (<u>PM₁</u>) CO: Model 48i
Japan	Noto (background)	137.36 °E, 37.45 °N	2011.01.01 – 2016.12.31	BC: MAAP ^b (<u>PM_{2.5}</u>) CO: Model 48i
	Fukuoka (suburban area)	130.47 °E, 33.52 °N	2014.09.01 – 2016.03.31	BC: MAAP (<u>PM_{2.5}</u>) CO: Model 48i

^a continuous light absorption photometer, ^b multi-angle absorption photometer

Table 2. Means and standard deviations of the black carbon (BC)^a, carbon monoxide (CO)^b, Δ CO concentrations^b, CO baseline^b, amount of APT^c and the number of data for all (N_{all}) and APT=0 ($N_{\text{APT=0}}$) cases at each site.

	All	Spring	Summer	Fall	Winter
(a) Baengnyeong					
BC	826.5 ± 304.4	855.8 ± 204.0	561.7 ± 149.7	795.3 ± 300.8	1017.9 ± 347.2
CO	293.8 ± 63.8	317.4 ± 40.0	242.6 ± 46.2	264.5 ± 59.8	339.0 ± 57.9
Δ CO	128.9 ± 46.5	121.1 ± 24.0	104.1 ± 48.7	116.8 ± 41.7	167.4 ± 43.1
<u>CO_{baseline}</u>	<u>164.9 ± 43.1</u>	<u>196.3 ± 25.9</u>	<u>138.6 ± 46.1</u>	<u>147.7 ± 40.0</u>	<u>171.6 ± 36.7</u>
APT	3.6 ± 9.1	2.8 ± 6.4	9.1 ± 16.1	2.8 ± 6.5	1.5 ± 3.7
N_{All}	3,828	1,155	764	669	1,240
$N_{\text{APT=0}}$	1,793	560	199	339	695
(b) Gosan					
BC	490.2 ± 168.4	659.4 ± 200.4	323.4 ± 92.3	454.6 ± 59.7	542.2 ± 94.8
CO	190.1 ± 49.5	225.9 ± 20.0	128.4 ± 38.5	178.9 ± 29.4	227.1 ± 23.2
Δ CO	81.6 ± 27.2	87.2 ± 15.9	53.8 ± 21.3	77.8 ± 22.2	107.7 ± 18.8
<u>CO_{baseline}</u>	<u>108.4 ± 29.4</u>	<u>138.7 ± 6.7</u>	<u>74.6 ± 28.2</u>	<u>101.0 ± 17.8</u>	<u>119.4 ± 9.7</u>
APT	6.4 ± 14.4	4.2 ± 10.3	15.1 ± 23.0	5.2 ± 10.5	1.8 ± 3.6
N_{All}	2,510	395	598	778	739
$N_{\text{APT=0}}$	950	185	100	343	322
(c) Fukuoka					
BC	676.5 ± 105.8	665.5 ± 73.4	571.4 ± 43.9	700.0 ± 157.6	715.0 ± 63.3
CO	305.7 ± 43.7	303.6 ± 27.0	251.6 ± 34.7	293.3 ± 36.1	346.5 ± 26.8
Δ CO	124.6 ± 33.3	100.0 ± 22.9	99.6 ± 7.0	125.3 ± 35.4	152.9 ± 24.2
<u>CO_{baseline}</u>	<u>181.1 ± 22.7</u>	<u>203.6 ± 5.0</u>	<u>151.9 ± 28.3</u>	<u>168.1 ± 8.8</u>	<u>193.6 ± 11.9</u>
APT	6.4 ± 13.4	7.2 ± 13.7	13.9 ± 20.5	6.0 ± 13.1	3.3 ± 7.5

N_{All}	1,435	286	206	427	516
$N_{APT=0}$	547	114	37	179	217
(d) Noto					
BC	244.6 ± 81.0	339.9 ± 45.3	201.7 ± 54.2	203.1 ± 57.7	233.6 ± 74.6
CO	176.9 ± 31.9	212.1 ± 17.9	148.4 ± 17.1	157.2 ± 20.4	189.9 ± 21.7
Δ CO	45.4 ± 10.7	48.9 ± 7.4	44.8 ± 11.9	42.0 ± 10.9	46.2 ± 11.7
<u>CO_{baseline}</u>	<u>131.4 ± 28.0</u>	<u>163.3 ± 16.2</u>	<u>103.6 ± 17.0</u>	<u>115.2 ± 12.8</u>	<u>143.7 ± 15.0</u>
APT	7.9 ± 14.6	7.2 ± 13.9	13.7 ± 20.3	7.9 ± 13.4	3.2 ± 4.3
N_{All}	6,089	1,482	1,468	1,574	1,565
$N_{APT=0}$	1,290	415	267	353	255

^a ng m⁻³; ^b ppbv; ^c mm

Table 3. (a) Regional $\Delta BC/\Delta CO$ ($\text{ng m}^{-3} \text{ppb}^{-1}$) ratios and emission rates of (b) BC and (c) CO (in Tg per year) over East Asia from various emission inventories.

	This study ^a	REAS 2.1 (2008)	EDGAR (2010)	MIX (2010)	CAPSS (2015)	ECLIPSE (2015)	KORUS V2 ^c (2016)	QA4ECV ^d (2016)
(a) $\Delta BC/\Delta CO$								
East China	6.8 ± 0.5	7.70	13.5	11.7		10.6		
North China	6.4 ± 0.5	10.0	21.1	12.8		13.4		
Northeast China	8.2 ± 0.7	11.8	12.9	11.9		13.2		
North Korea	7.2 ± 0.7	3.70	6.85	3.90	-	21.1		
South Korea	7.9 ± 1.2	23.2	7.68	35.6	25.1	10.6	17.8 ^e	14.5 ^e
Japan	6.8 ± 1.0	6.48	7.27	5.87	-	6.44		
(b) BC								
East China		0.400	0.329 ^b	0.416		0.382 ^b		
North China		0.331	0.215 ^b	0.360		0.355 ^b		
Northeast China		0.157	0.142 ^b	0.158		0.181 ^b		
North Korea		0.015	0.009	0.014	-	0.056 ^b	-	
South Korea		0.013	0.016	0.024	0.016	0.027 ^b	-	
Japan		0.026	0.023	0.020	-	0.019 ^b	-	
(c) CO								
East China		65.0	30.5 ^b	44.4		45.2		
North China		41.2	12.7 ^b	35.1		33.1		
Northeast China		16.6	13.8 ^b	16.6		17.1		
North Korea		5.14	1.55	4.49	-	3.30		
South Korea		0.69	2.56	0.84	0.79	3.18	0.90	1.10
Japan		5.03	3.97	4.28	-	3.66		

^a With uncertainty (1σ) calculated by regional and seasonal mean values.

^b Calculated based on administrative division from the emission inventory, which did not provide regional emission rates.

^c Based on the improved CAPSS for 2015 and CREATE v3 in China for 2015 using SMOKE-Asia emission processing at a 0.1° resolution

(Woo et al., 2012).

^d From multiconstituent data assimilation. Please find more details in Miyazaki et al. (2019).

^e Using the BC emission rate from the REAS 2.1 emission inventory

Supplement of

Regional variability in black carbon and carbon monoxide ratio from long-term observations over East Asia: Assessment of representativeness for BC and CO emission inventories

Yongjoo Choi et al.

Correspondence to: Yongjoo Choi (choingjoo@jamstec.go.jp)

S1 Seasonal variation in dominant emission regions

Figure S2 shows the seasonal variation in data frequency and total mean fraction of dominant emission regions when APT was zero (without precipitation). Depending on the geographical characteristics, there is a distinct pattern of dominant emission regions. We decided that the valid dominant emission regions would only be considered when the fraction of frequency was higher than 5% to ensure an adequate statistical analysis. As a result, Baengnyeong was suitable for monitoring the Chinese regions (East, North, and Northeast; 14–25%) and Korea (South and North; 8.1% and 16%, respectively), whereas Gosan was mainly influenced by the Chinese regions (11–20%) and South Korea (37%), along with a decreasing fraction of North Korea (4.2%). The Fukuoka and Noto sites were also good representatives for emissions from Japan (51% and 58%, respectively); however, Fukuoka was good for East and North China (12% and 9.3%) and South Korea (20%), and Noto was good for Northeast China (22%) and South Korea (7.1%).

S2 Dry deposition effects

The basic assumption in this analysis is that the BC concentration does not show a significant decrease due to dry deposition during transport from the main source region. Similar to Kanaya et al. (2016), we investigated the effect of dry deposition on BC particles from the main source regions to the receptor sites. Figure S3 is an example of a scatter plot between the $\Delta BC/\Delta CO$ ratio and traveling time at the Noto site, with the mean value of each five-hour bin less than 72 hours. The slope of the exponential best fit line is very low as $1.32 \pm 1.88 \times 10^{-3} \text{ hour}^{-1}$ (mean \pm 95% confidence interval) which is correspondence to 0.02 cm s^{-1} for the mean and 0.06 cm s^{-1} for the upper 95% confidence interval of dry deposition velocities when the mean mixing height was 646 m, as calculated by the HYSPLIT model. Not only the Noto site but also the other three sites also showed low dry deposition velocities within a range between 0.01 and 0.03 cm s^{-1} , suggesting that the assumption is valid.

S3 The variation in the $\Delta BC/\Delta CO$ ratio depends on the residence time

Since the $\Delta BC/\Delta CO$ ratio could be influenced by the residence time over the emission source regions, it should be investigated whether the variation in the $\Delta BC/\Delta CO$ ratio depends on the residence time in the same dominant emission region. Figure S4 shows the mean ratio with the standard deviation (vertical solid lines) divided by 20% intervals of the residence time fraction (total 73 hours) of the dominant emission region, along with a bar plot, which indicates the number of data for each bin. The open square symbols with a vertical dashed line indicate that the number of data was less than five (the 25th percentile of the number of data in each bin). We found that $\Delta BC/\Delta CO$ did not vary significantly according to the fraction of residence time when the number of data (N) was higher than five. The difference between each fraction in the same dominant emission region was statistically insignificant ($p > 0.05$), except for ‘South Korea’ in Fukuoka and ‘Others’ in Noto, when Welch’s t-test and the analysis of variance (ANOVA) were applied to two and more than two groups, respectively. This result indicated that the variation in the $\Delta BC/\Delta CO$ ratio according to the fraction (residence time) could be negligible when N exceeds five for the fraction of the residence time. Hereafter, we used the data that satisfied the threshold ($N > 5$) of each bin for comparison with the REAS emission inventory. To verify whether these results were caused by the influences of other emission regions, the dominant emission region was constrained by considering only direct influences without passing through other emission regions. Although the constrained $\Delta BC/\Delta CO$ ratios were only available for Korea and Japan, the mean ratios did not show a significant difference from the original ratio, implying that the effects of other emission regions were not significant.

S4S4 Uncertainty of regional and seasonal $\Delta BC/\Delta CO$ ratios

The $\Delta BC/\Delta CO$ ratio could be influenced by applying difference estimation methods for the CO baseline and altitude criteria for allocation of the dominant emission region. First, there are several ways to determine the CO baseline, mainly depending on the measurement period. For intensive measurement periods, the CO baseline can be calculated from the 5th percentile of data (Matsui et al. 2011; Miyakawa et al., 2017) or the x-intercept of the best-fit line between BC and CO (Oshima et al., 2012). It can also be calculated by the 5th percentile of the CO concentration from monthly (Verma et al. 2011) or moving 14-day (Kanaya et al. 2016) from long-term measurements. We tested the difference in CO baselines calculated from the 5th

percentile of the moving 14-day (our method) and monthly CO data (Figure S5). The difference in the CO baseline from the monthly data was slightly lower (-2 ppbv; -1.9%) than our estimation. Moreover, the mean $\Delta BC/\Delta CO$ ratios from the two different methods did not show significant differences ($5.82 \text{ ng m}^{-3} \text{ ppb}^{-1}$ for our estimation and $5.87 \text{ ng m}^{-3} \text{ ppb}^{-1}$ for monthly data), when Welch's t-test was applied ($p > 0.1$). Second, we also checked the difference in $\Delta BC/\Delta CO$ which can be caused by applying 1.5 km as a threshold to determine the dominant emission region. There was no significant difference in the regional $\Delta BC/\Delta CO$ ratios between 2.5 and 1.5 km when Welch's t-test was applied ($p \geq 0.1$). For the seasonal variation, though five cases (spring, fall and winter in East China, fall in North China and winter in Northeast China) of recalculated REAS BC/CO values showed significant differences ($p < 0.05$), the ratios of those cases varied within $\pm 1.4 \text{ ng m}^{-3} \text{ ppb}^{-1}$ ($\pm 15\%$), indicating that the MFBs were preserved. From these results, we confirmed the representativeness of our regional and seasonal $\Delta BC/\Delta CO$ analysis.

S5 Footprint for Northeast China

Although the backward trajectory for Gosan passed a similar region to that for Baengnyeong (Figure [S5S7](#)) and the difference in the $\Delta BC/\Delta CO$ ratio due to residence time was negligible, it was hard to exclude the possibility of mixing with emissions from South Korea from the beginning. The high $\Delta BC/\Delta CO$ in the low-residence time fraction for Northeast China in Gosan also supported the possibility of influence from South Korea (Figure S4).

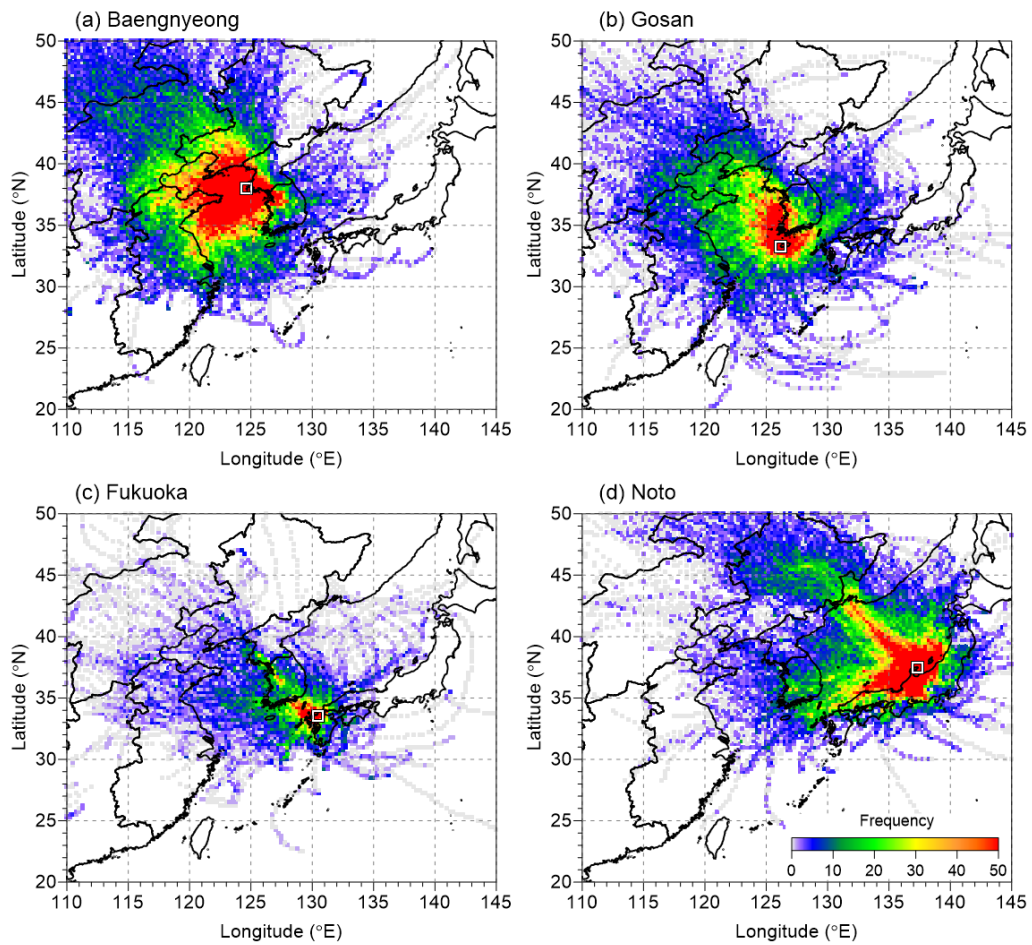


Figure S1. Footprint of the total number of backward trajectory endpoints for a $0.5^\circ \times 0.5^\circ$ grid cell depending on the measurement site.

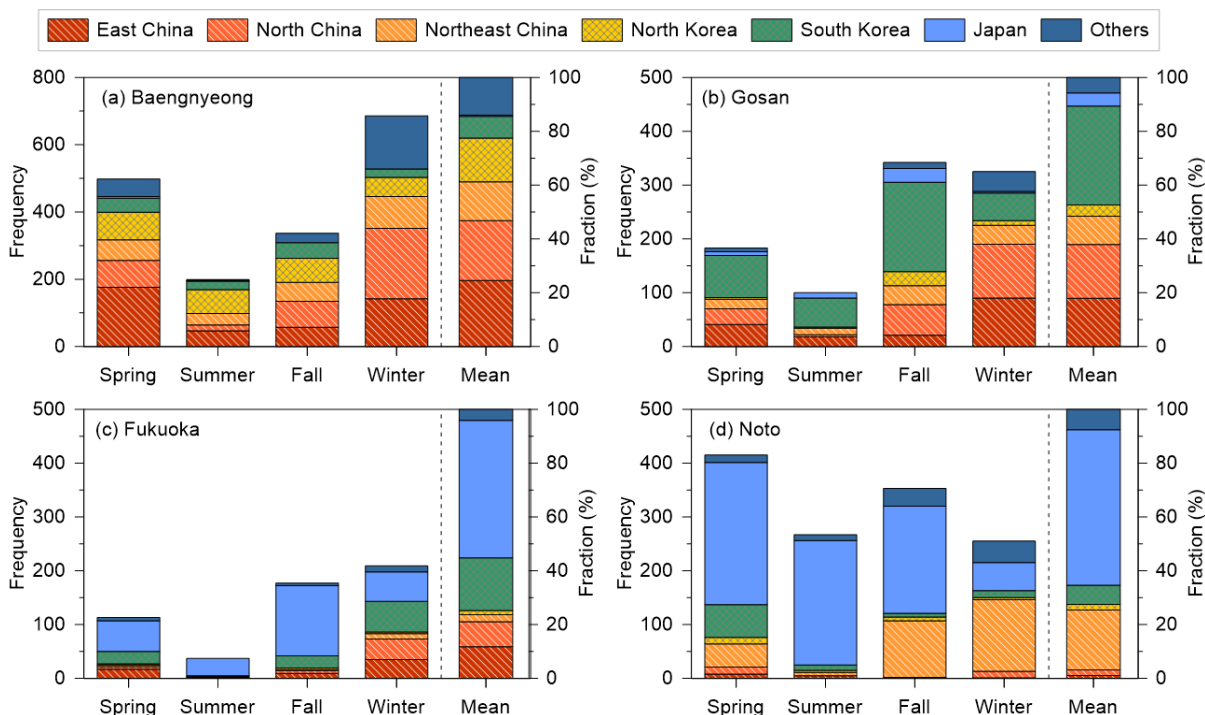


Figure S2. Seasonal variation in the frequency (left side of the dashed lines) and fraction (right side of the dashed lines) for backward trajectory-passed areas (dominant emission regions) in (a) Baengnyeong, (b) Gosan, (c) Fukuoka and (d) Noto.

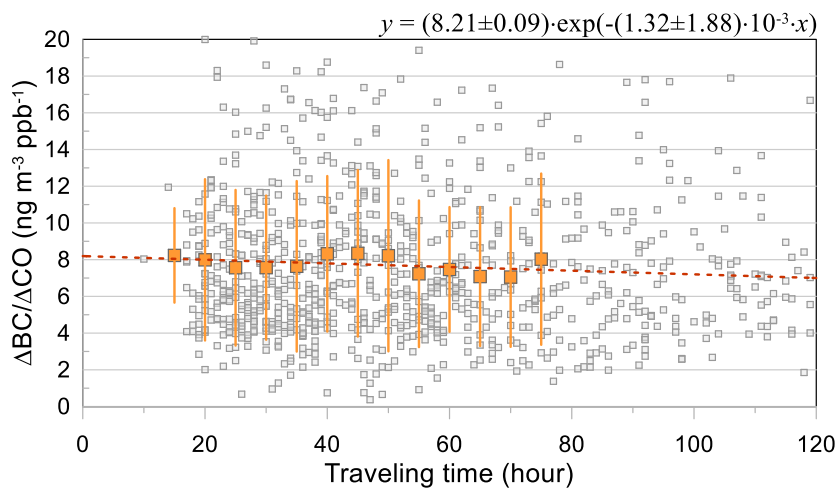


Figure S3. Scatter plot between the $\Delta BC/\Delta CO$ ratio and traveling time in Noto when the APT was zero. The gray squares indicate every observed data point, and orange squares with vertical lines represent the means and standard deviations of five-hour bins for less than 72 hours. The dashed line indicates the best-fit line.

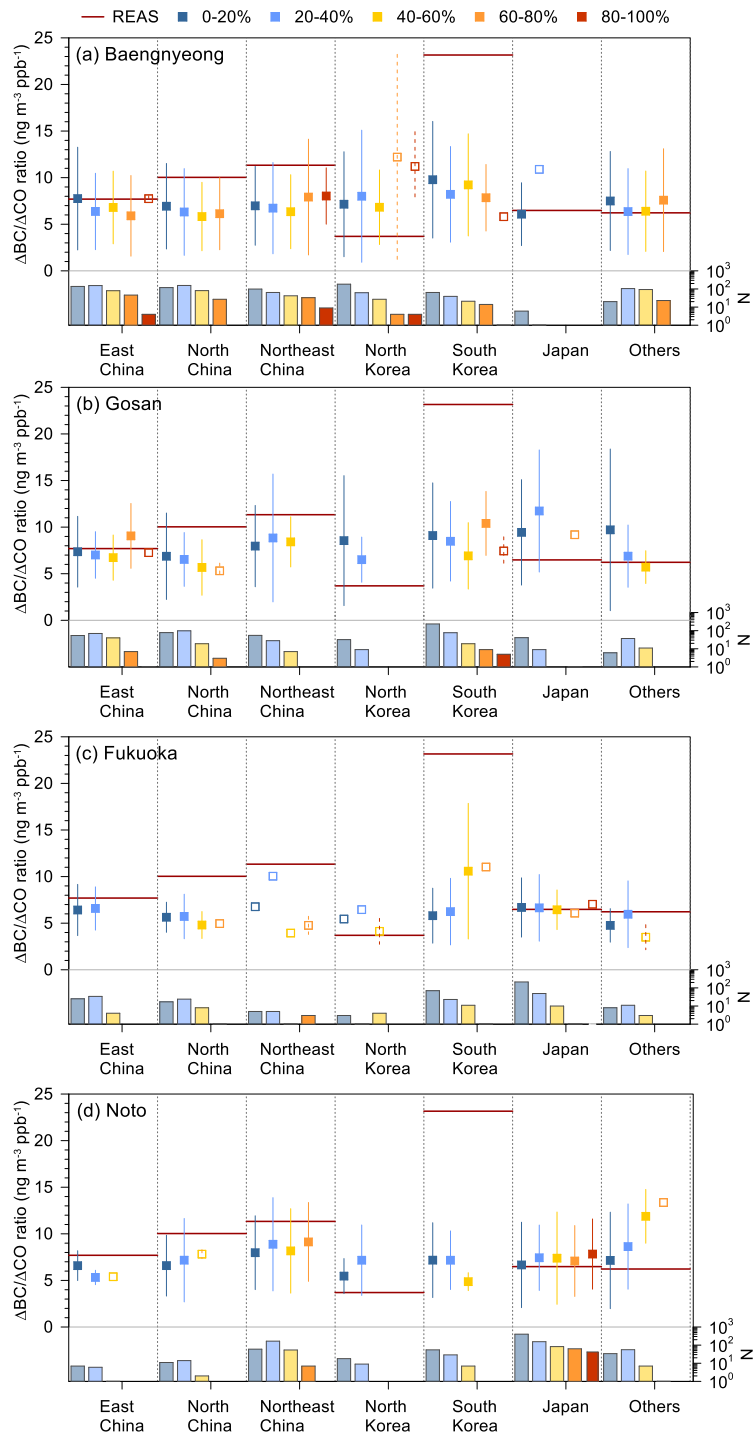


Figure S4. The measured $\Delta BC/\Delta CO$ ratios at four measurement sites depending on the residence time fraction in the dominant emission region. The colored symbols with solid lines and the open symbols with dashed lines indicate the mean and standard deviation of each bin for numbers of data ($N > 5$ and $N \leq 5$, respectively). The bar graphs on the bottom indicate the number of data in each bin and the dominant region. The horizontal red lines depict BC/CO ratios from the REAS emission inventory.

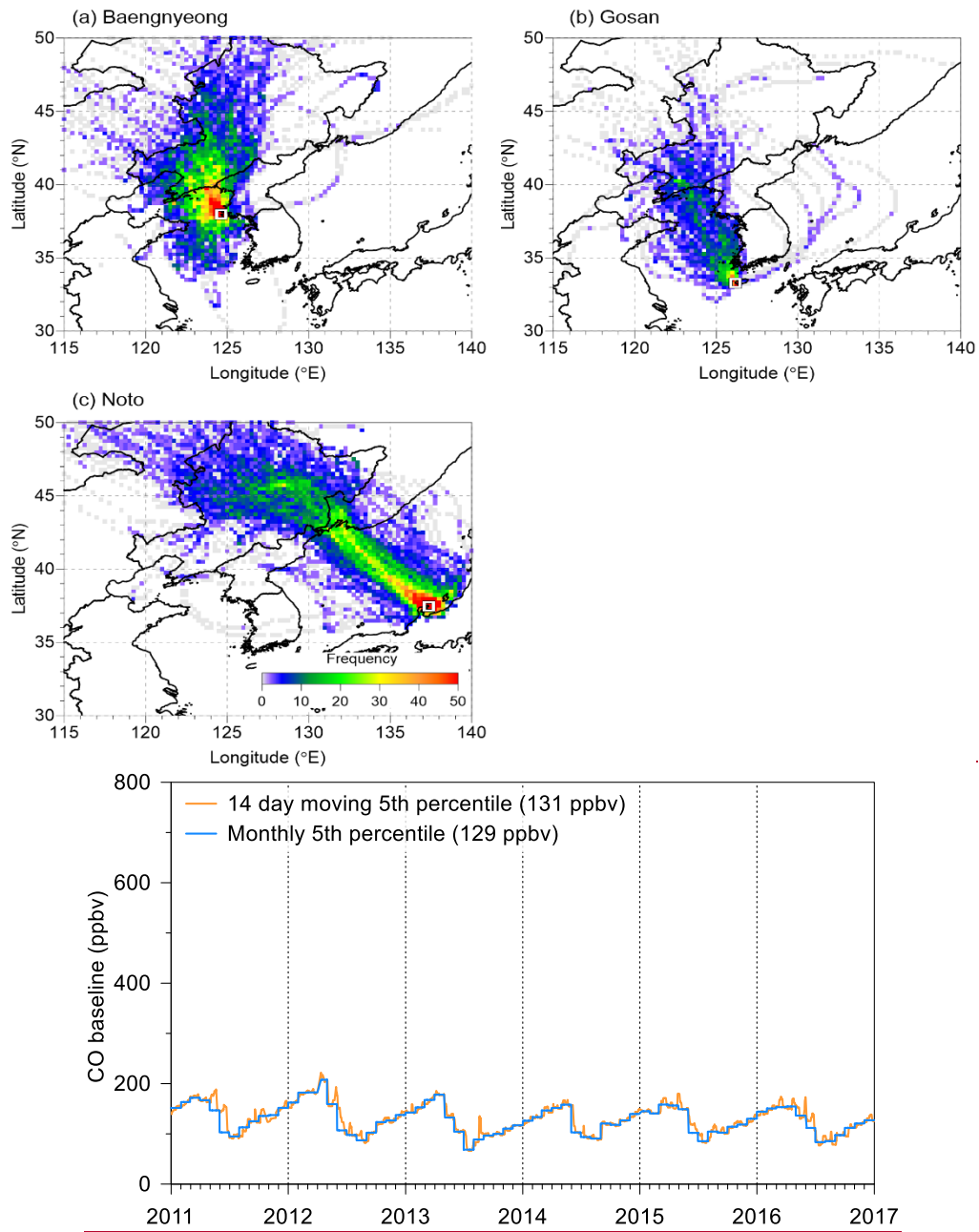


Figure S5. Time series of CO baselines calculated by different methods (14-day moving 5th and monthly 5th percentiles) at Noto.

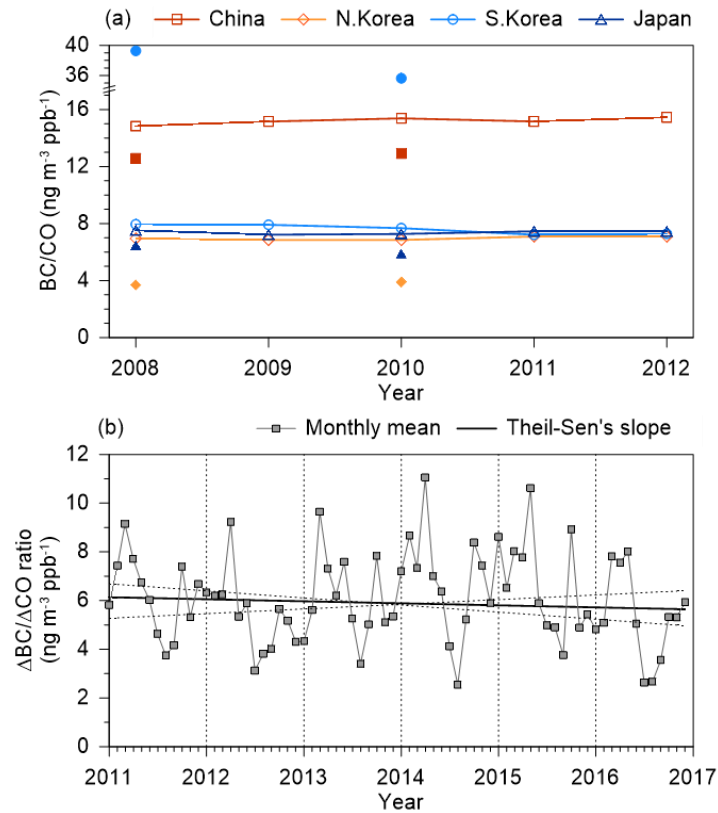


Figure S6. (a) Time series of the BC/CO ratios from the Emissions Database for Global Atmospheric Research (EDGAR v4.3.2; open symbols) during 2008 – 2012 and MIX emission inventory (filled symbols) in 2008 and 2010. (b) Time series of the monthly means of the $\Delta BC/\Delta CO$ ratio with Theil-Sen's slope during the measurement periods at Noto. The Theil-Sen's slope of the $\Delta BC/\Delta CO$ ratio indicated a slight decreasing trend of the $\Delta BC/\Delta CO$ ratio at $-0.08/\text{year}$; but the trend was statistically insignificant ($p > 0.1$). Insignificant trends of the $\Delta BC/\Delta CO$ ratio were also observed at the other sites.

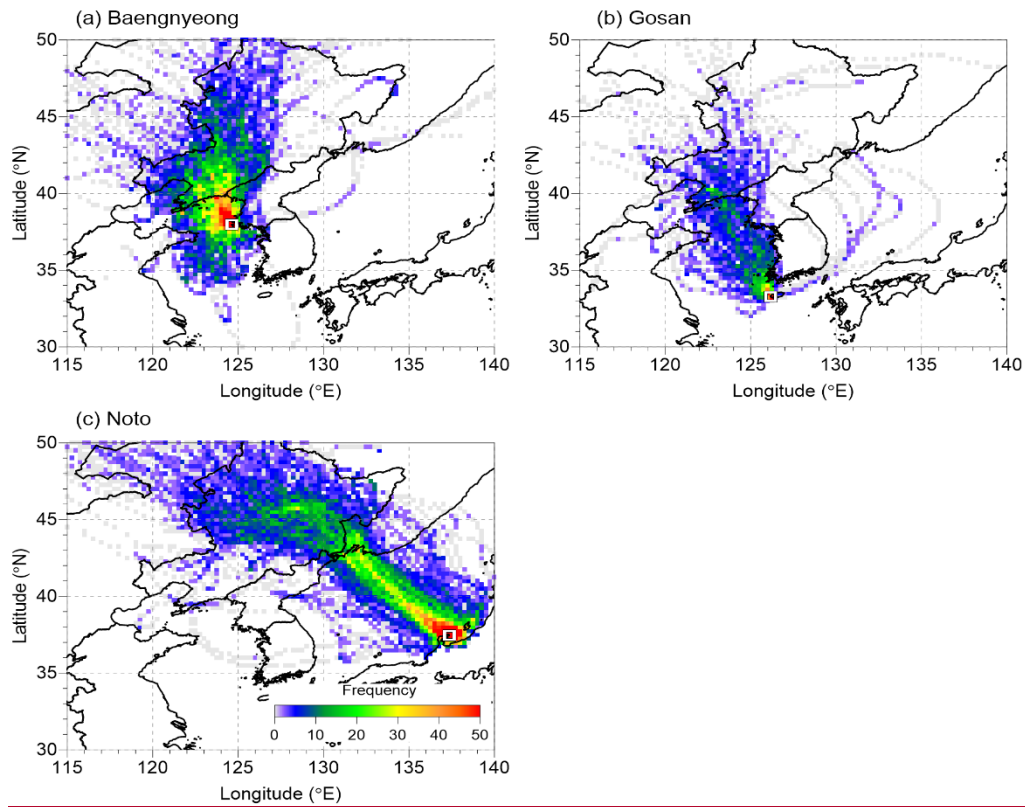


Figure S7. Same as Figure S1, except for the backward trajectory from Northeast China.

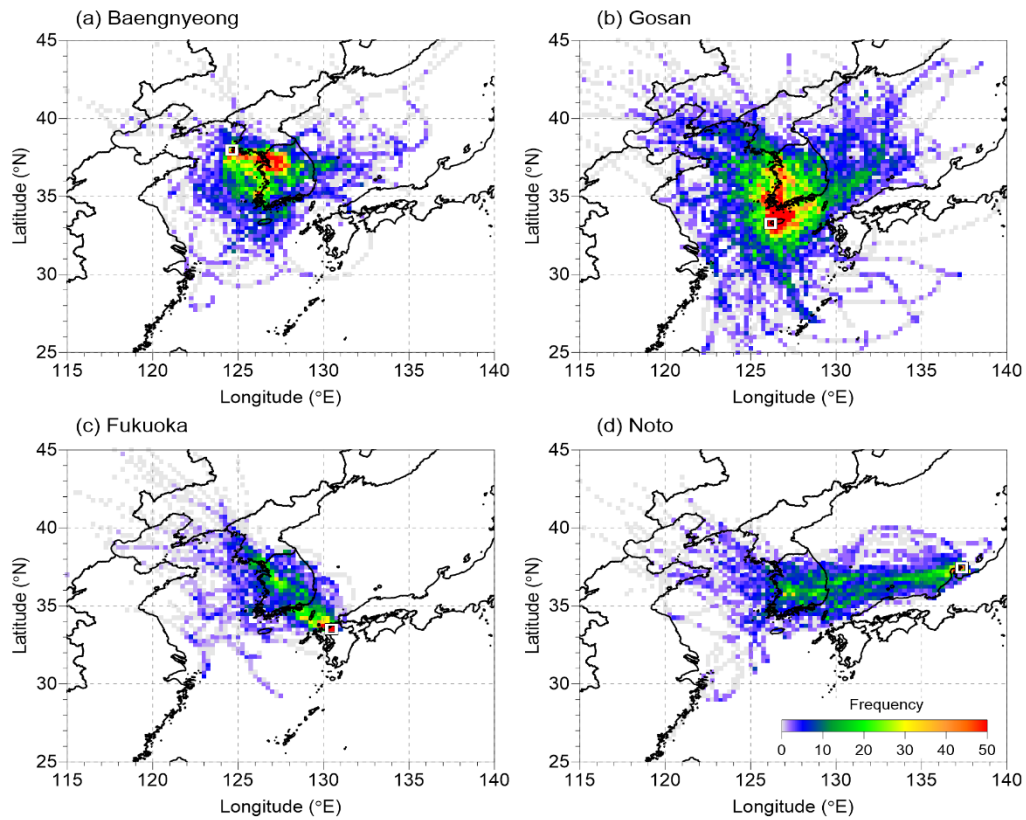


Figure S6S8. Same as Figure S1₁, except for the backward trajectory from South Korea.

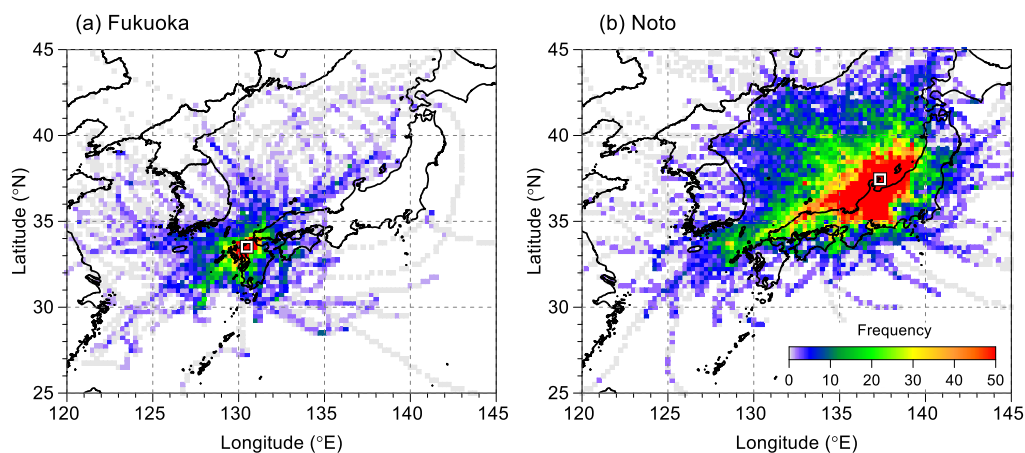


Figure S7S9. Same as Figure S1₁, except for the backward trajectory from Japan.

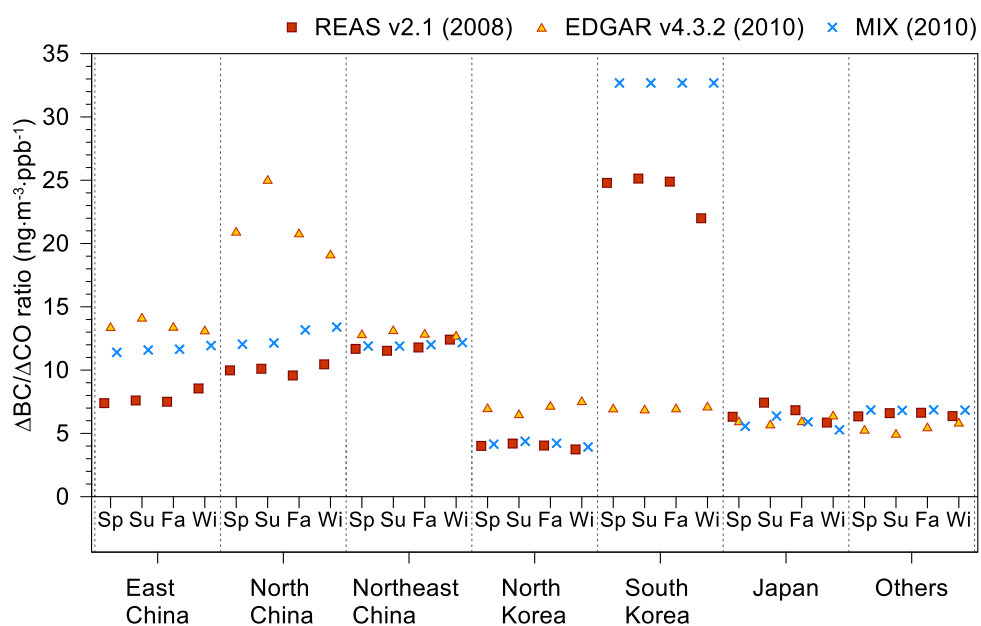


Figure S10. Seasonal variations of the overall regional mean BC/CO ratio according to different bottom-up emission inventories. The number in parentheses in each inventory indicates the base year. The abbreviation of ‘Sp’ to ‘Wi’ indicates spring to winter.